Title
Understanding the Spatial Variations of Pollutant Concentrations in Near-Road Environments

Author
Ranasinghe, Dilhara Roshini

Publication Date
2018

Peer reviewed|Thesis/dissertation

UNIVERSITY OF CALIFORNIA

Los Angeles

Understanding the Spatial Variations of Pollutant Concentrations in Near-Road Environments

A dissertation submitted in partial satisfaction of the

requirements for the degree Doctor of Philosophy

in Atmospheric & Oceanic Sciences

by

Dilhara Roshini Ranasinghe

2018

ABSTRACT OF THE DISSERTATION

Understanding the Spatial Variations of Pollutant Concentrations

in Near-Road Environments

by

Dilhara Roshini Ranasinghe

Doctor of Philosophy in Atmospheric & Oceanic Sciences

University of California, Los Angeles, 2018

Professor Suzanne E. Paulson, Chair

Many epidemiological studies have associated elevated concentrations of air pollutants found on and near roadways with a variety of adverse health outcomes. Concentrations of freshly emitted pollutants in urban areas exhibit a high degree of spatial variability, which makes pollutant exposures, and potentially their resulting health effects both very location dependent and difficult to estimate. Mobile air pollution monitoring offers an opportunity to map pollutants with much higher spatial resolution than sparse stationary monitors. In the first study, we developed a framework to address the challenges and constraints to developing higher spatial resolution maps from mobile data. For 1 s time resolution data collected at normal city driving speeds, we showed that concentration maps of 5 m spatial resolution can be obtained, by including up to 21% interpolated values. We estimated the minimum number of sampling runs needed to make a representative concentration map with a specific spatial resolution, and found that generally

between 15 to 21 repeats of a particular route under similar traffic and meteorological conditions is sufficient. The concentration maps can afford insights into factors influencing pollutant concentrations at the city block and sub block scale; information that is useful in urban planning strategies to reduce pollution exposure. Methodical analysis of mobile monitoring data facilitate meaningful comparison of concentration maps of different routes/studies.

Solid sound walls and vegetation barriers are commonly used to mitigate noise but they also help to reduce near-road air pollution. In the second study, we assessed the effectiveness of adding vegetation to sound walls (combination barriers) and vegetation-only barriers in reducing pollution concentrations downwind of roads. Using field measurements collected with a mobile monitoring platform, we developed concentration decay profiles of ultrafine particles, fine particles, oxides of nitrogen (NO and NO_2) and carbon monoxide downwind of two roads in California with different solid barrier-vegetation barrier configurations and meteorological conditions. Generally, when winds were blowing approximately perpendicular to the road, both vegetation and combination barriers were effective in reducing near road air pollution. Under calm and stable atmospheric conditions (wind speed < 0.6 m/s); a taller and denser vegetation-only barrier was more effective than a combination barrier. For ultrafine particles and gas pollutants, the additional reduction by vegetation-only barrier ranged from 10-24 %, in the first 160 m from the barrier. Under light winds (wind speed< 3 m/s), in both unstable and stable atmospheric conditions, combination barriers with moderately dense vegetation that is taller than the solid barrier were more effective relative to the sound wall or the taller and higher and denser vegetation barrier alone. The additional reduction by combination barriers ranged 6-33% in the first 160 m from the barrier. Our results are consistent with the notion that at low wind speeds vegetation act as effective barriers, and mean particle size data suggests a strong contribution of

deposition in reducing ultrafine particles downwind of vegetation barriers. At higher wind speeds, the importance of the barrier effect diminishes and their windbreak effect becomes more important. Overall, adding vegetation alone or to an existing solid barrier resulted in lower downwind pollution concentrations, especially under low wind speeds when concentrations are higher.

In the third study, we used a modified dispersion model "Quick Urban & Industrial Complex" (QUIC) together with field measurements to assess factors controlling the effectiveness of vegetation and combination barriers in reducing near-road pollution concentrations. Two study sites with different building morphologies and configurations of barriers were modeled using QUIC. QUIC simulations in general captured the effect of barriers on pollution dispersion and the complex flow in near-road urban environments. Improvements to handle characteristics of vegetation are needed to capture the wind speed dependent effects of vegetation barriers. The QUIC model showed promise as a useful tool to optimize the characteristics of barriers to mitigate near-road air pollution exposure.

The dissertation of Dilhara Roshini Ranasinghe is approved.

Marcelo Chamecki

Jochen Peter Stutz

Yifang Zhu

Suzanne E. Paulson, Committee Chair

University of California, Los Angles

2018

Dedicated to my father

Dayananda Ranasinghe

who taught me by example,

the resilience of the human spirit in adversity.

Table of Contents

List of Figures

List of Tables

Acknowledgements

First and foremost, I would like to thank my advisor Prof. Suzanne Paulson. Her support and guidance made my research a success, and her patience, understanding and kindness made my graduate school years memorable. Her thoughtful insights on both academic and personal issues helped me navigate graduate school life. I am sincerely grateful to her for believing in me and giving me the opportunity to be a part of her research group.

I would also like to thank my dissertation committee, Profs. Marcelo Chamecki, Jochen Stutz and Yifang Zhu, whose advice helped my research proposal and whose comments and suggestions greatly improved this thesis. I am also grateful for the support and friendship of past and present research group members, Dr. Wonsik Choi , Karen Bunavage, Isis Frausto, Dr. Michelle Kuang, David Gonzalez, Adlin Scott and Prof. Gisele Rocha.

The research projects were enriched by work conducted by our collaborators; Prof. J.R. DeShazo and Lisa Wu of UCLA Luskin School of Public Affairs, Prof. A.M. Winer and Dr. E. Lee of UCLA Fielding School of Public Health, Prof. A. Venkatram, Drs. S. Tan, S. Amini and F. Ahanga of UCR Mechanical Engineering, Prof. U. Seibt and Dr. W. Sun of UCLA Atmospheric Sciences and Mr. S. Mara and Drs. K. Kozawa, W. Ham, N. Schulte, T. Kuwayama of California air resources board.

I would like to thank all my friends at UCLA who made graduate school years fulfilling and my parents, sister and extended family who supported me through ups and downs in life. Finally, my heartfelt gratitude goes to my dear husband Amila for his unending love, friendship, support and patience. He inspired me to be a better researcher, he was my pillar of strength and stress reliever during difficult times and he was my reliable support team for field measurements and technical issues.

Vita

Dilhara Roshini Ranasinghe

Summary

An atmospheric scientist with research experience in urban air pollution, conducting research on spatial variation of air pollution in near-road environments and optimization of mitigation strategies to reduce pollution exposure in near-road communities.

Experience

- Expertise in urban air quality and in designing, planning and conducting field measurement campaigns
- Experience in mobile air quality measurements using a variety of particle and gas measurement instruments
- Experience in air quality data analysis, spatiotemporal data analysis
- Experience using QUIC dispersion model for air quality assessment
- Experience in formulating policy recommendations based on scientific research

Employment

Graduate student researcher, Dep. of Atmospheric & Oceanic Sci., UCLA June 2013-June 2018

Graduate teaching fellow, Dep. of Atmospheric & Oceanic Sci., UCLA January 2013-June 2017

Graduate teaching assistant, Dep. of Physics & Astronomy, UCLA Fall 2012

Teaching assistant, Dep. of Physics, Uni. of Peradeniya, Sri Lanka 2010-2011

Education

M.S., Atmospheric & Oceanic Sciences / University of California Los Angeles 2012–2014

B. S., Physics / University of Peradeniya, Sri Lanka 2006–2010

Publications

Choi, W.S., **D. Ranasinghe**, J.R. DeShazo and S.E. Paulson. "Where to locate transit stops: Cross-intersection profiles of ultrafine particles and implications for pedestrian exposure." *Environmental Pollution* (2018).

Eon S. Lee**, Dilhara R. Ranasingh**, Faraz Enayati Ahangar, Seyedmorteza Amini, Steven Mara, Wonsik Choi, Suzanne Paulson, Akula Venkatram and Yifang Zhu. "Field Evaluation of Vegetation and Noise Barriers for Mitigation of Near-Freeway Air Pollution under Variable Wind Conditions Atmospheric Environment." *Atmospheric Environment* (2018).

Dilhara R. Ranasinghe, Wonsik Choi, Arthur M. Winer, and Suzanne E. Paulson. "Developing High Spatial Resolution Concentration Maps Using Mobile Air Quality Measurements." *Aerosol and Air Quality Research* (2016).

Choi, Wonsik, **Dilhara Ranasinghe**, Karen Bunavage, J. R. DeShazo, Lisa Wu, Rodrigo Seguel, Arthur M. Winer, and Suzanne E. Paulson. "The Effects of the Built Environment, Traffic Patterns, and Micrometeorology on Street Level Ultrafine Particle Concentrations at a Block Scale: Results from Multiple Urban Sites." *Science of the Total Environment* (2016).

Presentations

Dilhara Ranasinghe, Isis Frausto-Vicencio, Eon Lee, Yifang Zhu, Seyedmorteza Amini, Faraz Enayati Ahangar, Akula Venkatram, Steve Mara, Suzanne Paulson, " The Effect of Sound Wall-Vegetation Combination Barriers on Pollution Dispersion from the Freeways" (poster presentation). *American Association for Aerosol Research Annual Conference, Portland OR, October 2016.*

Dilhara Ranasinghe, Isis Frausto-Vicencio, Wonsik Choi, Eon Lee, Yifang Zhu, Faraz Enayati Ahangar, Akula Venkatram, Seyedmorteza Amini, Steve Mara, Suzanne Paulson," Effectiveness of Road-side Vegetation and Noise Barriers on Reducing Ultrafine and Fine Particulate Matters under Variable Wind Speeds" (platform presentation). *Special Symposium on Passive mitigation strategies to reduce exposure to near-road air pollution, American Association for Aerosol Research Annual Conference, Raleigh NC, October 2017.*

Honors and Awards

Dissertation Year Fellowship, University of California Los Angles 2017

Brian Bosart Graduate Student award, Department of Atmospheric & Oceanic Sciences, University of California Los Angles 2016

B.S. First Class Honors, University of Peradeniya, Sri Lanka 2009/2010

University Award for Academic Excellence, University of Peradeniya, Sri Lanka 2009/2010

1. Introduction

Roadway combustion emits a suite of air pollutants including coarse (PM10-2.5; particle diameter between 10-2.5 μm), fine (PM2.5; particle diameter less than 2.5 μm) and ultrafine (PM0.1, UFP; particle diameter less than 0.1 μm) particles; carbon monoxide (CO); nitrogen oxides (NO_x); black carbon (BC); polycyclic aromatic hydrocarbons (PAHs) and volatile organic compounds (VOC). Numerous air quality studies show that compared to urban background levels concentrations of these pollutants are elevated, and in some cases highly elevated, on and near heavily trafficked roadways. An estimated 30-45% of people in large North American cities live within zones highly impacted by traffic emissions, covering up to 300-500 m from a highway or a major road (Health Effects Institute Panel on the Health Effects of Traffic-Related Air Pollution, 2010).

Many epidemiological studies have associated elevated concentrations of air pollutants found on and near roadways with a variety of adverse health outcomes including asthma and other respiratory diseases (Rice et al., 2014), birth and developmental defects (Stingone et al., 2014), premature mortality (Caiazzo et al., 2013), cardiovascular diseases (Chen et al., 2013) and childhood cancers, such as leukemia (Boothe et al., 2014). Children appear to be particularly vulnerable to these adverse effects of air pollution (Health Effects Institute Panel on the Health Effects of Traffic-Related Air Pollution, 2010).

In order to estimate the exposure of a population to air pollutants and to develop strategies to mitigate pollution exposure in near-road environments, we require a thorough understanding of the factors contributing to the spatial variation of pollution concentrations in those environments. The spatial and temporal variability of pollutant sources (primarily vehicles), microscale

meteorology and characteristics of natural and built environments are some of the important factors controlling the spatial variation of pollution.

Measurements of traffic-related pollutant concentrations in urban areas have shown large inter- and intra-community variations. Choi et al. (2013) reported that difference in UFP number concentrations could be as high as 260 % between urban neighborhoods just 4 km apart. In near-road environments, the distance for elevated pollutant concentration levels near roadways to return to the background levels show large variabilities associated with local meteorology (Finn et al., 2010), pollutant type (Karner et al., 2010) and roadway configurations (Heist et al., 2009). In the daytime unstable atmospheric conditions, the elevated pollution levels can extent up to 115-570 m on the downwind side of the freeways (Karner et al., 2010). In the night and early morning stable atmospheric conditions, the elevated pollution levels can extend much further, up to 2 km on the downwind side of the freeway (Choi et al., 2012).

Turbulent diffusion is one of the main mechanisms responsible for the rapid decrease of pollution concentration with increasing distance from the roadways. Air parcels with high pollution concentrations are mixed with background air, and the resulting concentration reduction pattern depends on the magnitude of the increase of pollutant concentration above its background level. A meta-analysis by Karner et al. (2010) revealed that pollutants can be generally put into two categories based on their concentration reduction patterns downwind of the road; ones that show a rapid decrease (>50% in 150 m) and the ones that show a gradual or less rapid decrease of the elevated concentrations. UFP number concentration, CO and BC concentration fall into the first category, showing a rapid decay and the relative concentrations of these three species track each other well (Zhu et al., 2002), while benzene, NO_2, PM2.5 fall into the second category, showing a gradual decrees in concentrations.

Coagulation, deposition, evaporation and condensation of semi-volatile species also contribute to the reduction of pollution concentrations (Zhang et al., 2004). For particles, these mechanisms are size dependent and more pronounced with decreasing particle size, as smaller particles have a higher molecular diffusion coefficients and dynamics of their evaporation are more pronounced due to the Kelvin effect (Hinds, 1999).

In urban areas, built environments can form complex airflow patterns, such as street canyon flows, channeling flows and corner vortexes that can contribute to large spatial variability in pollution concentrations (Buonanno et al., 2011; Pirjola et al., 2012; Choi et al., 2016). These studies emphasize the importance of considering pollutant concentration variations at fine spatial scales, and the potential to reduce exposures to roadway emissions via adjustments to the built environment.

Recognizing the negative impacts from near-road pollution exposure, new laws and mitigation strategies have been implemented to reduce the exposure of near-road communities. Some of the widely considered mitigation strategies for exposure reduction are limitations on placing sensitive land uses such as residences, schools, day care centers, playgrounds and medical facilities at close proximity to freeways, dynamic traffic management using air quality forecasts, optimization of noise barriers, roadside vegetation and road vegetation together with catalytic coatings, road surface cleaning and dust binders.

The work presented here has three main objectives: 1) to develop a methodology to produce high spatial resolution concentration maps using mobile air quality measurements and estimate number of repetitions of mobile measurement runs needed to make representative UFP concentration maps with high spatial resolution (chapter 2); 2) to assess the effectiveness of vegetation and combination barriers in reducing near-road pollution concentrations (chapter 3) and 3) to use the

QUIC dispersion model to probe factors controlling the effectiveness of vegetation combination barriers as a pollution mitigation strategy.

2. Developing High Spatial Resolution Concentration Maps Using Mobile Air Quality Measurements

2.1 Introduction

An increasing number of air quality studies use mobile air pollution monitoring. Mobile measurements have several advantages over conventional stationary measurements, including the opportunity for better data coverage, efficient collection of data in close proximity to sources and logistical efficiency (Hagler et al., 2010; Hagler et al., 2012; Hu et al., 2012; Birmili et al., 2013; Choi *et al.*, 2013;Peters et al., 2013; Van Poppel et al., 2013; Brantley et al., 2014; Lähde et al., 2014). Although mobile measurement data can be highly spatially resolved, they are not always presented as high spatial resolution concentration maps. Many studies have presented either data statistics or aggregated data for streets or route segments (Hagler et al., 2010; Hagler et al., 2012; Hu et al., 2012; Choi *et al.*, 2013; Peters et al., 2013; Van Poppel et al., 2013). Taking advantage of the high spatial resolution of the data offers potential to identify spatial variations and local air pollution hot spots at sub-block scale resolution, which in turn can provide exposure estimates for near-road communities, pedestrians and transit users to elevated levels of pollution near roadways. A detailed understanding of exposure risks could influence urban planning strategies such as placing transit stops and businesses with outdoor seating away from local pollution hot-spots, as well as behavioral changes such as choosing walking routes with minimal pollution exposure.

Recently several studies have presented concentration maps of mobile measurement data (Pirjola et al., 2012; Padró-Martínez et al., 2012; Brimili *et al.*, 2013; Brantley *et al.*, 2014; Lähde et al., 2014; Pattinson et al., 2014; Peters et al., 2014). Pirjola et al. (2012), Lähde et al. (2014) and Padró-Martínez et al. (2012) do not state the spatial resolution of their maps, and provide little

description of how the maps were developed; Padró-Martínez et al. (2012) utilized ArcGIS 9.3.1 to develop concentration maps for individual runs. Brantley *et al.* (2014) and Pattinson et al. (2014) used 1 s time resolution data together with ArcGIS (ESRI) to map the median values of sets of runs and produced 50 m spatial resolution maps. The data along the measurement routes were binned into segments of 50 m and circles of 50 m diameter by Brantley *et al.* (2014) and Pattinson *et al.* (2014), respectively. Birmili *et al.* (2013) took an important step towards preserving the high spatial resolution of the 10 s time resolution mobile monitoring data collected by walking, a configuration that produced data with one measurement roughly each 8 m. They found systematic divergence of global positioning system (GPS) coordinate data from the walking path, and after correcting for this divergence, allocated data into ± 5 m horizontal segments. Their resulting UFP number concentration measurements were presented as maps with 10 m spatial resolution, where each data point was the geometric average of the data from 38 runs. Peters *et al.* (2014) used a large set of 1 s time resolution data collected using a bicycle as a mobile monitoring platform (MMP), a configuration that produced data with roughly one measurement each 3.2 m. The GPS data were corrected using linear interpolation for short time periods when the GPS data were missing. Data were then projected on to the street based on shortest distance between the data point and the cycling route. The measured particle concentrations were spatially aggregated based on a Gaussian weighting function to produce concentration maps with 10 m spatial resolution.

The main issues encountered in developing high spatial resolution concentration maps from mobile monitoring data are (i) the non-uniform spatial resolution and distribution of the measurements; (ii) that measurements are made at slightly different locations in each measurement pass along a specific route (in each "run") and in some cases; (iii) errors in GPS coordinate data, which are common in dense urban areas with tall buildings. Additionally, there is the question of

how much data is sufficient to provide reliable profiles. The selection of the spatial scale for data aggregation and averaging must be informed by the spatial resolution of the collected data. In practice, the spatial resolution of the collected mobile measurement data is a combined result of the instantaneous speed of the MMP and the sampling rate/time resolution of the instruments used. Unlike for mobile measurements collected by walking or cycling for which the speed of MMP can be kept somewhat uniform, for motor vehicle MMPs large irregularities in the travel speed are unavoidable, especially in urban traffic. Consequently, even when instruments sample at a constant rate, the spatial resolution of data can be non-uniform, making the production of high resolution concentration maps challenging.

When the time resolution of the data set is varied due to the nature of either the instrument or the post-data-processing procedures, determining the spatial resolution of collected mobile measurement data becomes more complex. An example of introduced spatio-temporal variability is the BC measurements made with micro-aethalometers, which can use an optimized noise-reduction averaging algorithm (ONA) that prescribes a varying averaging time (Van den Bossche et al., 2015). However, because variations due to post-data-processing procedures is rare, the spatial resolution of mobile measurement data and consequently the highest possible spatial resolution of mobile measurement concentration maps are often limited by the combination of the data sampling rate and the instantaneous speed of the MMP.

Here we propose solutions to the above mentioned mobile air quality data processing issues using a reference grid to map data points, and a piecewise cubic Hermite spline interpolation between measurements to give equal weight to each sampling run at each grid reference point. A background correction can be used to facilitate averaging concentration data over different days/times. Finally, we address the issue of how many repetitions of mobile measurement runs are needed to make

representative UFP concentration maps with high spatial resolution.

2.2 Measurements

The data used in this study are from a field campaign conducted in and around Downtown Los Angeles (DTLA). This campaign is described in more detail in Choi et al. (2016) and is only briefly described here. The site considered here is a 2-by-2 block area centered on the intersection of Broadway and 7th Street (BW-7th) (34°2'42.70"N/118°15' 12.23"W). The area consists of densely packed commercial buildings and parking structures, and a fairly typical street canyon configuration with a building height/street width (aspect ratio) of about 1.7. The block lengths are 190 m and 100 m and the street widths are 26 m and 22 m for BW and 7th streets, respectively. The BW-7th intersection has a tall building at each of the four corners, with median height of 46 m. The mean building height for the site area is 34 m and the building heights range 3–60 m (Fig. 1).

Measurements of several traffic-related air pollutants including UFP number and size distribution, PM2.5, black carbon, particle bound poly-aromatic hydrocarbons (PB-PAH), NO, CO, and CO_2 were collected using fast response instruments fitted inside a MMP, an electric sub-SUV free from self-pollution (Table 1). The instruments in the MMP have different response times due to the characteristics of the instruments and differences in inlet length and flow rates. Air was drawn through a 6" diameter galvanized steel manifold installed through a window of the rear passenger space located 1.5 m above ground level. Sampling ports for each instrument were located in the middle of the manifold with short (0.5–2 m) sampling tubing (1/4" Teflon for gases, 1/4" conductive tubing for particles, and 1/2" conductive tubing for FMPS).

Fig. 1 The sampling route of the mobile monitoring platform (MMP) in downtown Los Angeles. BW denotes Broadway and EB, WB, NB, and SB represent eastbound, westbound, northbound and southbound, respectively. Map source: Google Earth.

For each instrument, flow and zero checks were performed before and after each measurement session. To account for any slight day-to-day differences in response time, a time-lag correlation method was used in post-data processing to synchronize the response time of the instruments (Choi et al., 2012). Concentration data and MMP position data were recorded at 1 s time resolution. A complete description of the MMP calibration procedures is available in Hu et al. (2009).

Table 1. Monitoring instruments on the mobile monitoring platform.

Instrument	Measurement Parameter	Response time[a] (Inlet to record)
TSI Portable CPC, Model 3007	Sub-micrometer particle number count (10 nm–1 μm)	*4 s*
TSI FMPS, Model 3091	Size-segregated particle count (5.6–560 nm)	*9 s*
TSI DustTrak, Model 8520	$PM_{2.5}$ Mass	*5 s*
EcoChem PAS 2000	Particle-bound PAH	*10 s*
Teledyne API Model 300E	CO	*21 s*
LI-COR, Model LI-820	CO_2	*7 s*
Teledyne-API Model 200E	NO	*22 s*
Magee Scientific Aethalometer AE42	Black Carbon	*21 s*
Vaisala Sonic Anemometer and Temperature/RH sensor	Surface winds, temperature, and relative Humidity (*RH*)	-
Garmin GPSMAP 76CS	Location and speed	-
Eurotherm Chessell Graphic DAQ Recorder	Data-logger	-

[a] Response time is an averaged value for smoke test results (Choi *et al.*, 2013 (S3)).

The MMP was driven multiple times along a fixed route (Fig. 1). Each day two data collection sessions were conducted, one in the morning (07:00–10:00) and one in the afternoon (14:00–17:00) with 6–9 and 6–7 runs in the morning and afternoon, respectively (Table 2). MMP turns at intersections were recorded in a time log. The MMP was parked intermittently at various locations for 5 min periods to collect meteorological data from its sonic anemometer mounted on the roof of the MMP. In each measurement session, video recordings of traffic were made at the central intersection using cameras mounted at each of the four corners of the intersection. Detailed information on the traffic signal light changes and traffic counts for all four traffic flow directions were obtained manually by reviewing the video records. All data processing was done in MATLAB R2012a (The Mathworks, Inc.).

Table 2. Measurement periods and surface meteorology at BW-7th.

Date	Measurement Period	BW			7th		
		Wind speed ($m\ s^{-1}$)	Wind direction#	Traffic flow (vehicles s^{-1})	Wind speed ($m\ s^{-1}$)	Wind direction#	Traffic flow (vehicles s^{-1})
7/1/2013	09:15–11:45	0.96	SW	0.09	*1.08*	ESE-NE*	0.15
	15:30–18:00	0.91	SW	+	+	+	+
7/3/2013	08:15–11:00	*1.34*	SSE–SW*	0.10	1.06	ESE–NE*	0.13
	16:00–18:00	*1.80*	SW–S*	0.18	1.45	NE	0.18
7/5/2013	08:45–11:00	*1.23*	*	0.95	0.94	ESE–NW*	0.08
	15:30–18:15	*1.13*	SSW–NW*	0.14	1.48	NE	0.14

NE (northeasterly), ESE (east-southeasterly), SSE (south-southeasterly), S (southerly), SSW (south-southwesterly),
SW (southwesterly), NW (northwesterly).
* variable wind (wind direction was spread over two or more quadrants).
+ data not available.

2.3 Data Analysis Methodology

The UFP number concentrations measured using the CPC had the lowest response time (Table 1) and consequently highest spatial resolution, making it the best data set for concentration variations at a high spatial resolution. Therefore, we present the data analysis methodology using CPC measured UFP number concentrations.

2.3.1 Separation of the High-Emitting Vehicle Contribution

Transient concentration spikes from high-emitting vehicles (HEV) are common on roadways. HEV encounters have a strong stochastic element and the associated concentration spikes can deviate as much as 1–2 orders of magnitude above the baseline. As HEV data have the potential to obscure general trends in concentration maps, depending on the question being asked,

it may be desirable to remove them.

Here HEV encounters occurred 10 to 14% of the time, depending on the session, defined as follows. To identify HEV-related spikes, a threshold concentration value must be defined. The method developed by Choi et al. (2013) was used here, in which a site- and session-specific threshold was calculated. The threshold concentration value was defined as the baseline plus three standard deviations of the baseline. First, we subtracted a baseline calculated using a robust smoothing function that employs a local regression of weighted linear least squares and a 2nd degree polynomial model. The smoothing function assigns lower weight to outliers in the regression and assigns zero weight to data outside six mean absolute deviations. Next, the standard deviation of the baseline-subtracted concentrations was calculated. Then all concentrations above this intermediate threshold of three standard deviations were identified as HEV spikes and removed from the data set. A new standard deviation was calculated from the remaining concentration data, resulting in a new threshold. The process was iterated eight times, until the threshold value converged to a constant value. All concentration values above the calculated final threshold were replaced by the baseline concentration values to obtain the final HEV spike-removed concentration time series used for certain analyses.

2.3.2 Correction of Geographical Data

Handheld GPS units are able to obtain coordinates with a horizontal accuracy of approximately 3–5 m when the unit can receive a wide area augmentation system (WAAS) signal. Otherwise, the accuracy is approximately 10–15 m. In urban settings with tall buildings, shadowing effects can result in poor reception of satellite signals (Misra & Enge, 2006) and further decrease position accuracy. In our dataset the GPS data diverged by up to about 30 m from the roadway at times, almost exclusively under slow moving or stationary conditions. This is similar

to the divergence reported by Birmili et al. (2013). Often near street corners, the GPS data appeared in clusters or gave sets of position data implying backward movement (Fig. 2).

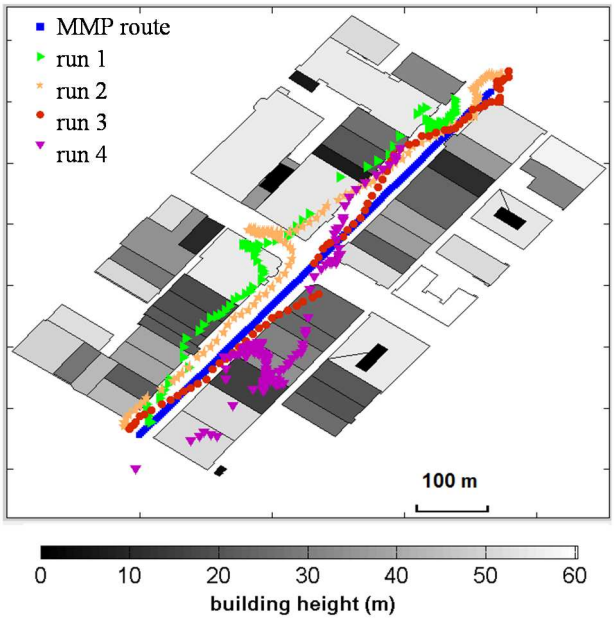

Fig. 2 An example of the divergence of GPS data in an urban street canyon. The color dots show the position data of four runs, obtained from GPS device (Garmin GPSMAP 76CS) while driving along Broadway Northbound. The blue squares denote the reference line; a close representation of the actual driving route of the MMP during the data collection.

GPS data were corrected as follows. A time log of the instant the MMP turned at each intersection was used to divide both concentration and position data time series into street segments. Clusters of position data implying backward movement were identified by comparing GPS data to latitude/longitude values along the diving route. As these 'wandering' data clusters were most pronounced under slow moving or stationary conditions, all the concentrations associated with such a set of positions were attributed to the last position which showed a forward movement.

2.3.3 Handling Non-Uniform Spatial Resolution of Measurements

To achieve the objective of developing representative mean concentration maps with high spatial resolution, data averaging should be performed in a manner that does not overweight or underweight any of the data. Initially we adapted an areal average (Hagler et al., 2010; Pattinson et al., 2014) in which values with in a fixed radius were averaged for data points along the route. For example, if a radius of 4 m was chosen, all points within an 8 m diameter circles were averaged and assigned to the center of the circle. This approach proved to be erroneous at small spatial scales because a large number of data points associated with large divergences of GPS data were excluded.

In a novel approach to handling the non-uniform spatial resolution of mobile monitoring data, we first constructed reference lines to provide a framework with which to organize the data. For one way streets, the reference lines were assigned to the mid-line of the street, and for two lane streets the reference lines were assigned to the mid-line of all the lanes in a single direction. These reference lines provided the framework and acted as placeholders to produce concentration maps at different spatial resolutions.

As described earlier, in practice the spatial resolution of the concentration data is related to the instantaneous speed of the MMP. The average speed of the MMP was about 3 ms^{-1} for all sessions, with a standard deviation of 2.9 ms^{-1} and 3.4 ms^{-1} for morning and afternoon sessions, respectively. This average MMP speed is comparable to the 3.2 ms^{-1} reported by Peters et al. (2014) for bicycling (with 1 s resolution instruments) but is much faster than the 0.8 ms^{-1} reported by Birmili et al. (2013) for walking (with 10 s resolution instruments). Fig. 3 shows that about 80% of the time the MMP traveled at speeds below 5 ms^{-1}, corresponding to a spatial resolution at or above 5 m. However, lower spatial resolution data tend to be clustered in certain areas, such

as low trafficked streets and at the middles of the blocks. Based on this understanding of the variation of the spatial resolution of data, we decided to look at spatial scales ranging from 2 m to 40 m and investigated the implications of the choice of spatial scale in data aggregation and averaging.

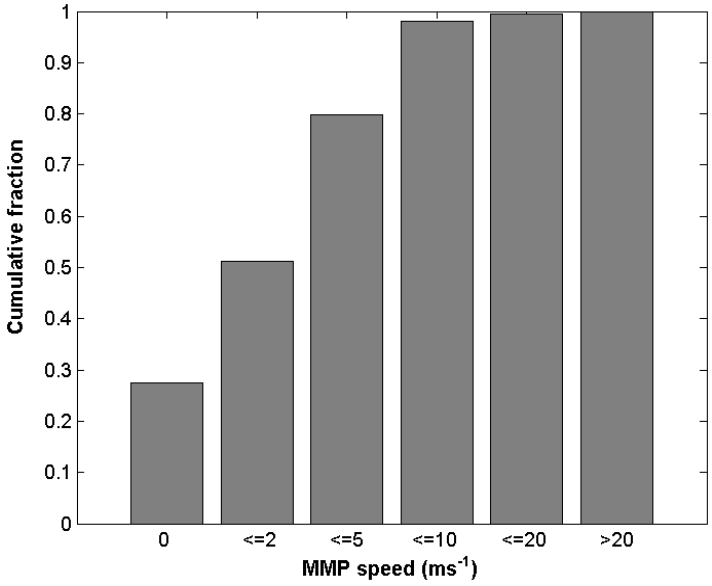

Fig. 3 Cumulative fraction of the binned instantaneous speed of the mobile monitoring platform (MMP), calculated for the whole dataset including both morning and afternoon sessions.

After the correction of GPS data, each data value for each run was assigned to the closest line reference point along a particular street. After this step, runs typically have some line reference points with no assigned values and others with many values. In cases where multiple data values were assigned to a reference point for an individual run, the mean of the assigned values was calculated. The rationale for averaging these data points is to not to over-weight the MMP stops. In the dense urban area of our study, street lights spend equal amounts of time as red and green (with a brief yellow phase), but the MMP naturally collects more data while stopped at a red light,

sometimes as much as 50 times the data collected when it passes through an intersection on a green light. Thus averaging the extended measurements from the red phase gives appropriate weighting to the green and red phases. Not surprisingly, as the spatial resolution of the reference lines was increased, the number of reference points with no assigned data values increased. These empty reference points present a problem because they cause over-weighting of the runs that did produce data at a particular reference point. This problem can have a dramatic effect, producing plots that are very noisy. Over-weighting a run is particularly concerning if that run is influenced by a transient emission event. Further, as the urban background concentration (see definition in section 2.3.4) varies throughout a measurement session, a run that is missing data at a given reference point results in a temporal bias toward the time periods in which runs are available at that point.

As a solution to these biasing issues, to assure the availability of a concentration value at each reference point for each run, the concentration data within individual runs were interpolated at points where a data value was missing for that run. For this interpolation the Piecewise-Cubic-Hermite-Interpolation scheme (PCHIP) was selected. PCHIP uses a third degree polynomial specified in Hermite form to produce a smooth continuous function of the concentration time series (Fritsch & Carlson, 1980). The piecewise calculation not only keeps the calculation 'local' using only four neighboring data points, but also avoids the oscillations in the interpolated data that are associated with higher order polynomial interpolations. Fig. 4 show that the PCHIP scheme preserves the concentration time series well for individual runs.

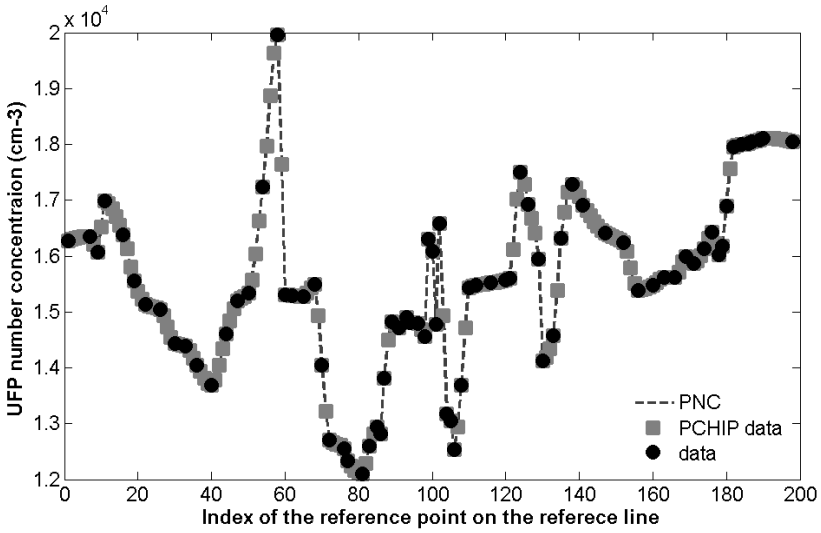

Fig. 4 An example of the interpolation of concentration data values for an individual run at 2 m spatial resolution. 'Data' points (circles) represent observed concentration values. 'PCHIP data' points represent the interpolated concentration values (squares). Note that the maps shown in Fig. 6 use 5 m resolution and thus fewer interpolation points than this example.

An investigation of the percentage of interpolated data values required at different spatial scales shows that concentration maps of 4 m spatial resolution can be obtained by including 32% interpolated values; this number falls to 4% for 10 m spatial resolution (Fig. 5). The percentage of interpolated data allowed suggests an upper-bound for the spatial resolution of concentration maps. Considering the horizontal accuracy of the GPS position data is about 3–5 m and that the PCHIP scheme preserves the within-run concentration time series well, we choose to allow up to 21% of values to be interpolated, and present concentration maps with 5 m spatial resolution. Once each run has an appropriate single data value assigned at each reference point, the runs are averaged together to create the desired concentration maps.

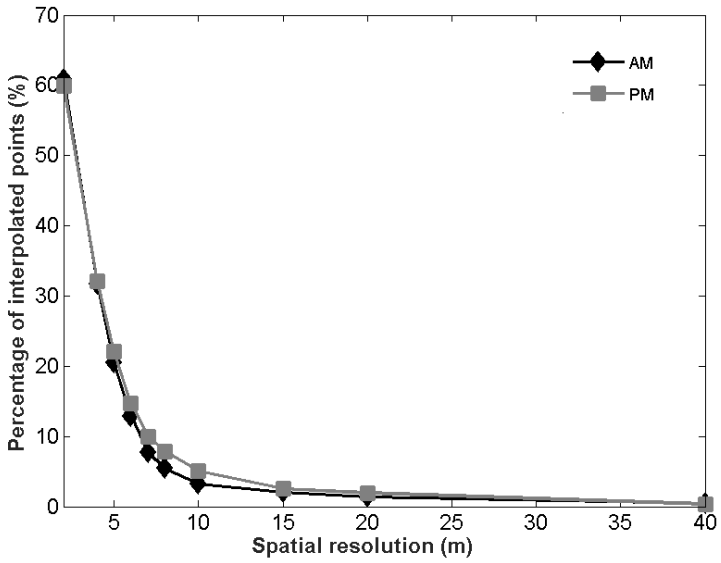

Fig. 5 The percentage of interpolated points in the data set used to calculate the mapped concentration as a function of spatial resolution of the reference lines, for data with 1 s time resolution and mobile monitoring platform mean speed of about 3 ± 3 m s^{-1}.

2.3.4 Estimation of the Urban Background

Day to day and within several hours on the same day, average pollution concentrations often move up and down by a factor of two or more, due to large scale phenomena such as mixing height and turbulence intensity, as well as general traffic trends. These variations in the urban background must be accounted for prior to averaging data from different sessions and days. The urban background can be defined as the ambient air pollution concentration that does not show transient variations due to local sources (Brantley et al., 2014). Background estimation techniques fall into two main categories: location-based estimates such as the use of a background site, and time-series based estimates such as the use of a low percentile of the data, the rolling minimum over small time windows, a spline over the minimums or low percentiles of small time windows of the time series. The efficacy of these different techniques and the dependence of time series-based estimates on the width of the time window were discussed extensively in Brantley et al.

(2014). They concluded the time series based background estimate that best captured the diurnal and daily variations was a spline over the minima of reasonably narrow time windows, and that the choice of a 5 min or 10 min time window does not make a significant difference. Their study showed that for UFP concentrations, the time series-based background estimates using a spline over minimums (after removing background zones from the time series) and the location-based estimate of the median of a background zone were in good agreement.

Here we obtained a time series-based background estimate by fitting a smooth function to the minimum values in 10 min time windows for each morning and afternoon session. By subtracting the spline of minimum values from the measured concentration values, the background-subtracted concentration time series were obtained. This resulted in approximately 6.8% negative values in the concentration time series, which is comparable to the 7.3% reported by Van Poppel et al. (2013) for a location based background correction method.

Background-subtracted time series from different days can be averaged to produce mean concentration maps to probe spatial variations. However, such maps do not represent the measured concentration values, only their variability. To address this issue, a representative urban background can be added back to provide exposure estimates. The percentage contribution of the background to the measured concentration, calculated using the ratio of mean of background time series to the mean of measured time series, was 33% and 26% for morning and afternoon sessions, respectively. This is comparable with an all session average of 26% reported by Brantley et al. (2014). In order to make the background corrected concentrations representative of the measurements, we averaged the estimated background splines for different sessions and added the resulting mean background spline to each background-subtracted concentration time series to obtain the background-adjusted concentration time series. These background-adjusted

concentration time series from different days were used together with corrected GPS data to assign concentration values to the reference grid points and then data within individual runs were interpolated at points where a data value was missing for that run, as described in section 2.3.3. Next, all runs from several days were averaged (morning and afternoon sessions separately) to obtain the mean concentration maps (Fig. 6).

2.3.5 Micrometeorological parameters

The sonic anemometer measurements (Table 1) were used to calculate several micrometeorological parameters related to surface turbulence. The along-wind (U), mean cross (V) and vertical (W) components of the wind measurement at time t, can be expressed in terms of the mean wind for a given period ($\overline{u}, \overline{v}, \overline{w}$) and the fluctuation of the wind at time t (u', v', w')(Eq. 1).

$$\begin{aligned} U &= \overline{u} + u' \\ V &= \overline{v} + v' \\ W &= \overline{w} + w' \end{aligned} \qquad \text{(Eq. 1)}$$

Then the mean fluctuations of vertical winds (σ_w), friction velocity (u^*) representing a velocity scale for the total vertical flux of horizontal momentum and the mean turbulence kinetic energy (TKE) are given by Eq.2,3 and 4, respectively (Stull 1988).

$$\sigma_w = \sqrt{\overline{w'^2}} \qquad \text{(Eq. 2)}$$

$$u_*^{\,2} = \sqrt{\overline{u'w'}^2 + \overline{v'w'}^2} \qquad \text{(Eq. 3)}$$

$$TKE = \frac{1}{2}\left(\overline{u'^2} + \overline{v'^2} + \overline{w'^2}\right) \qquad \text{(Eq. 4)}$$

2.4 Results and Discussion

2.4.1 High Spatial Resolution Concentration Maps

2.4.1.1 Ultrafine particles

The 5 m spatial resolution maps shown in Fig. 6 are the result of careful consideration of several underlying data processing issues of mobile monitoring data. With the use of a background correction, we were able to average data over sessions from different days, and thus over a higher number of runs. After averaging data over varying effects of micro-meteorology, traffic volume, traffic fleet composition and background concentrations over different measurement sessions and different days, resulting UFP concentrations maps retain the robust block and sub-block scale features of the concentration variation, making them a potentially useful tool in identifying pollution hot spots at the block or sub-block scale (Choi et al., 2018).

Fig. 6 shows the UFP concentration maps at 5 m spatial resolution for the full data set including HEV-related spikes ("raw", Figs. 6(a) and 6(c)) and also for the data with HEV-related spikes removed ("spikes removed", Figs. 6(b) and 6(d)). The dominant feature of the "raw" concentration maps are the 'hot spots' that appear at and near intersections, including both the area where queues form and where vehicles accelerate away from intersections. Once the HEV related spikes are removed, features appear that reveal more about the influence of the built environment on street level concentrations. While "raw" concentration maps are important in exposure analysis, maps with HEV spikes removed help understand various other factors influencing small spatial scale variations of the UFP concentration.

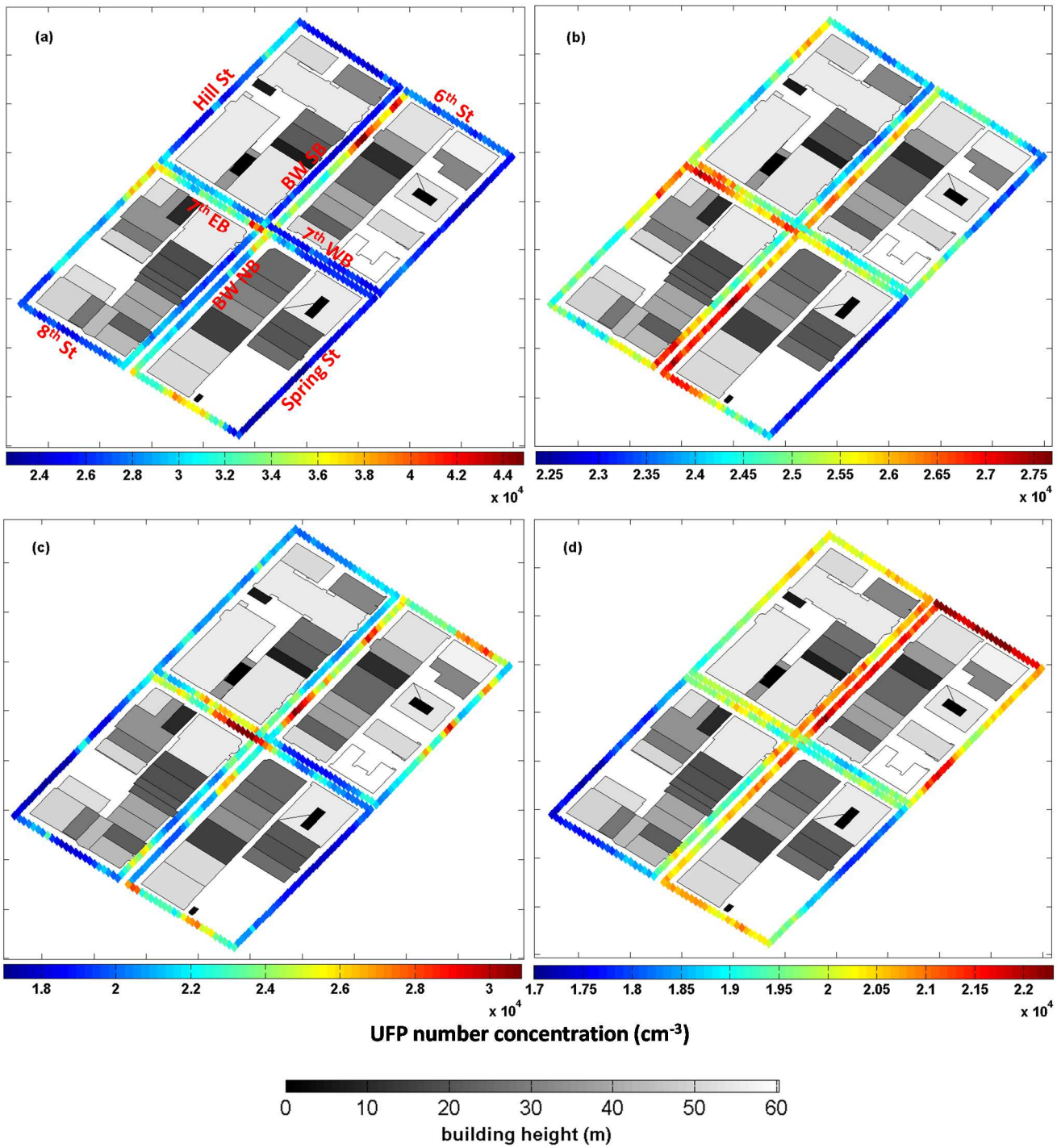

Fig. 6 Spatial variations of background corrected UFP concentrations averaged over (a,b) morning and (c,d) afternoon sessions from three days for (a,c) data including HEV related spikes and (b,d) data excluding HEV related spikes. The spatial resolution of the maps is 5 m.The heights of the buildings in the nearby area is shown in gray scale.

The "spikes removed" data reveal features at both the block- and sub-block scales. Fig. 6(d) shows that at the block-scale, in the afternoon, 6th street shows the highest concentrations, despite having low average traffic volume compared to other streets. On 7th street, in both morning and afternoon, there are generally higher concentrations on the east-bound side compared to the west-bound side, despite having nearly the same traffic flow in both directions. Moreover, Fig. 6(b) shows that at the sub-block scale, in the morning on BW northbound near the intersection of 8th and BW, the south end of the block has elevated concentration in comparison to the queue forming north end. A similar situation can be noted on 8th street, just west of the intersection of BW and 8th, where the east end of the block shows elevated concentration in comparison to the queue forming at the west end. Many of these features can be explained by the surface level wind flow patterns that are heavily influenced by the local built environment, traffic patterns and non-vehicle local sources (Choi et al., 2016).

2.4.1.2 Gas pollutants

We chose to demonstrate the mapping methodology using UFP because UFP measurements have the potential to show the heterogeneity of the spatial distribution of the pollutants in high spatial resolution maps. However, the internal averaging times of all the instruments were on the same order of magnitude (Table 1) and the concentration data for all the pollutants and MMP position data were recorded at 1 s time resolution. Given that the time resolution of the concentration data set and geographical data set is the same for all the pollutants, the mapping methodology considering the geographical data correction and handling of the non-uniform spatial resolution of measurements apply directly to the mapping of any of the pollutants.

Below we present examples of concentration maps of pollutants other than UFP. For each pollutant, the data-procession methodology described in section 2.3 was used to produce concentration maps at 5 m spatial resolution (Fig. 7 and Fig. 8). However, we emphasize that the instruments used to measure CO and NO have internal averaging times substantially longer than the 1s associated with the UFP measurements (Table 1). This means the underlying data do not capture a true signal change at 5 m spatial resolution. Additionally, their concentrations deviate less relative to UFP above the urban background. Both of these factors result in concentration maps that show with lower spatial heterogeneity than for UFP.

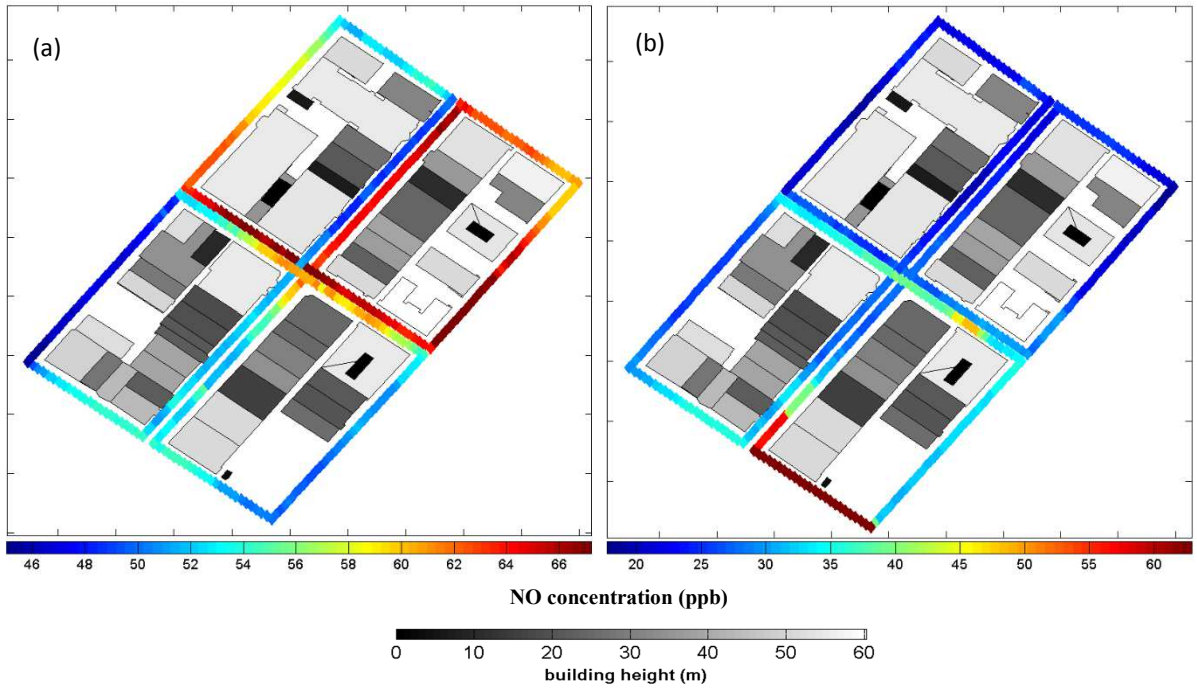

Fig. 7 Spatial varation of background corrected NO concentrations avaraged over (a) morning and (b) afternoon sessions from three days for data including HEV related spikes.The spatial resolution of the maps is 5 m.The heights of the buildings in the nearby area is shown in gray scale.

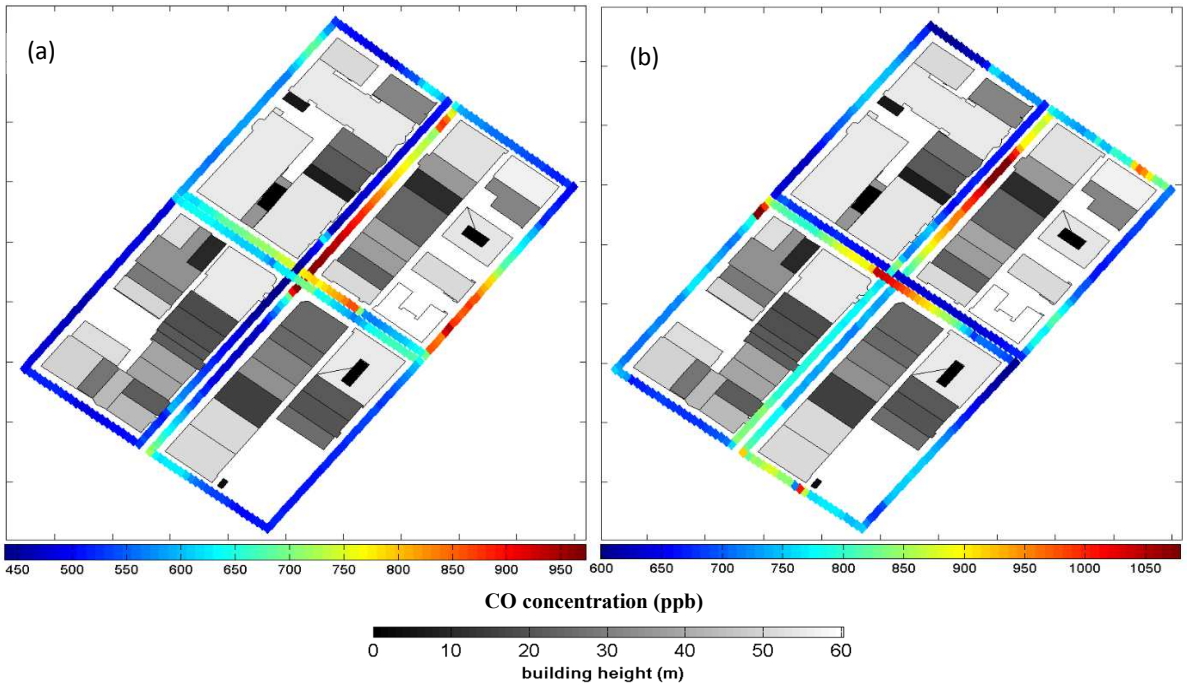

Fig. 8 Spatial varation of background corrected CO concentrations avaraged over (a) morning and (b) afternoon sessions from three days for data including HEV related spikes.The spatial resolution of the maps is 5 m.The heights of the buildings in the nearby area is shown in gray scale.

2.4.2 Estimation of the Minimum Number of Runs Needed for Representative Concentration Maps

Due to transient and small spatial scale variations in pollution concentrations, a single run of mobile measurements is clearly unable to capture a representative concentration field of an area. This raises the question of how many repeated measurements are needed to estimate a representative concentration field. Clearly this question is dependent on variability in meteorological as well as traffic conditions, features that in some cases might require very large amounts of sampling. Here we are interested in typical morning and afternoon conditions that, in the case of our study site, are the most common by far. The average wind speeds on BW were 1.2 ± 0.2 ms^{-1} for mornings and 1.3 ± 0.5 ms^{-1} for afternoons. The most prevalent wind direction on

BW was SW in both morning and afternoon sessions. On 7th the average wind speeds were 1.0 ± 0.1 ms^{-1} for mornings and 1.5 ± 0.1 ms^{-1} for afternoons. The most prevalent wind directions on 7th were ESE in the mornings and NE in the afternoons (Table 3). To investigate this question, the following data experiment was performed on the UFP number concentration data set.

Table 3. Average surface meteorology at BW-7th. Here, $u_*$is the friction velocity, σ_w is the variance of vertical wind velocity and TKE is the turbulent kinetic energy*.

Date	Temp. (°C)	u_* (m s^{-1})	σ_w (m s^{-1})	TKE (m^2 s^{-2})	Temp. (°C)	u_* (m s^{-1})	σ_w (m s^{-1})	TKE (m^2 s^{-2})
	Morning				Afternoon			
7/1/2013	25.9	0.23	0.37	0.47	32.2	0.23	0.40	0.46
7/3/2013	23.0	0.17	0.35	0.47	22.5	0.36	0.57	0.97
7/5/2013	20.6	0.19	0.30	0.47	24.0	0.15	0.48	1.21

* The definitions of micrometeorological parameters are presented in section 2.3.5.

First, all morning runs and all afternoon runs from the background-corrected concentration data set were collected separately. Each of these sets had runs spanning several days; many with fairly similar meteorological and traffic conditions (Table 2). For mornings, up to 22 runs were available for BW south-bound and 7th east-bound and 24 runs for BW north-bound and 7th west-bound. For afternoons, up to 19 runs were available for BW south-bound and 20 runs for other streets. For each street, at each line reference point, runs were selected at random (without replacement) and the mean concentration was calculated using an increasing number of runs, up to one less than the total number of runs available. This process was repeated 10 times for each street, choosing runs in different random order. For the sets of 10 repeated mean concentration calculations at different reference points and for different number of runs averaged, the relative error (standard deviation normalized by mean) was calculated and plotted (Fig. 9(a)). As shown in

Fig. 9(a), the rate of decrease in relative error varies among reference points along a given street. For simplicity, the maximum relative error along each street is considered and plotted against number of runs averaged for HEV spikes removed data (Fig. 9(b)) and for HEV spikes retained data (Fig. 9(c)). The minimum number of runs needed for the relative error to drop below 0.15 is calculated (the green or yellow symbols on each plot in Fig. 9(b) and (c)) and considered as the minimum number of runs needed for a representative UFP concentration value.

The estimate of the minimum number of runs needed for representative UFP concentration values at 5 m spatial resolution varies somewhat from street to street and is dependent on the data filters applied (Fig. 9 (b) and (c)). For HEV spikes removed data, the maximum relative error along each street vs. number of runs averaged (Fig. 9(b)) initially drops rapidly (in the first 2–7 runs). The maximum relative error along streets also drops rapidly initially, from the initial values of 282–90% to 50% at 4–9 runs, after which it decreases more slowly, reaching 15% at 15–21 runs. Hence, the estimate of the minimum number of runs needed for representative concentrations at 5 m spatial resolution ranges 16–21 runs for the mornings and 15–16 runs for the afternoons (Fig. 9(b)). For mornings when 16 runs are included, the average relative error considering all four streets is 11%. For afternoons when 15 runs are included, the average relative error considering all four streets is 9%. The morning sessions usually have low wind speeds (Table 3). Consequently, the turbulent kinetic energy (TKE) and variance of vertical wind velocity (σw) are lower in the mornings in comparison to the afternoons (Table 3), denoting lower atmospheric turbulence and mixing rates. The need for more runs for the morning sessions can be attributed to the lower mixing rates, resulting in a stronger influence of local sources on pollutant concentrations.

The inclusion of transient and large HEV spikes generally increases the minimum number

of runs needed for all the streets and for both AM and PM sessions (Fig. 9(c)). Similar to the HEV spikes removed data, morning sessions need more runs compared to afternoon sessions. For HEV spikes retained data, the maximum relative error along each street vs. number of runs averaged drops slowly compared to HEV spikes removed data. The maximum relative error along streets also drops from the initial values of 244–143% to 50% at 8–14 runs and drops below 15% only 5 sessions out of the 8 sessions. For all the streets maximum relative error along the streets drop below 22% at 21–23 runs for the mornings and for 17–18 runs for the afternoons. Hence we conclude that the of the minimum number of runs needed for representative UFP concentrations at 5 m spatial resolution is at least 21–23 runs for the mornings and at least 17–18 runs for the afternoons.

These results apply only to UFP concentrations because the minimum number of run needed for representative concentration values depends on the magnitude of variance of the data set. Hence the results depend on the pollutant considered. We also showed that the results depend on the data filters applied (Fig. 9(c)). The effect of spatial resolution on the estimate of the minimum number of runs needed for representative concentration values is discussed in section 2.4.3. For both HEV spikes removed and spikes retained data sets, the initial values of the maximum relative error markedly decreased when spatial resolution was decreased to 10 m. The minimum number of runs needed for representative concentration values generally decreased for all the streets and for both AM and PM sessions.

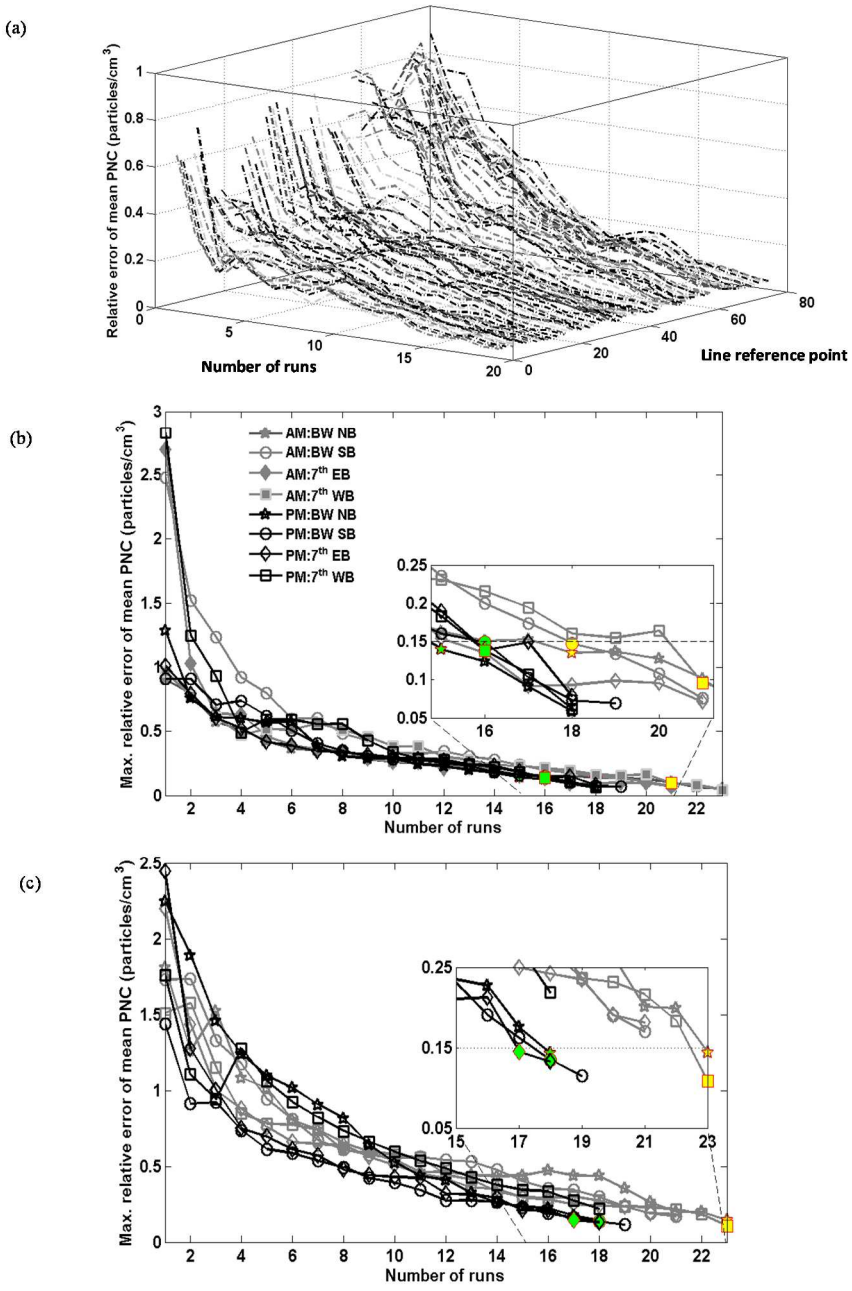

Fig. 9. (a) The relative error of repeated calculations of mean concentration of HEV spike removed data, for different numbers of averaged afternoon runs included in the averaging (x-axis), at each line reference points along a single example street (BW SB) (y-axis). (b, c) The variation of maximum relative error along different street segments vs. the number of runs averaged for morning (AM) and afternoon (PM) sessions (b) for HEV spikes removed data and (c) for HEV spikes retained data. The green and yellow symbols denote the points at which the relative error is at or below 0.15. The spatial resolution of the maps considered is 5 m.

In their effort to assess the minimum number of runs needed for representative concentrations at the street-scale, Van Poppel et al. (2013) and Peters et al. (2013) used data from moderately sized sets of mobile monitoring runs (20–24 runs), selecting different numbers of runs at random (without replacement) and averaging them to calculate the street means or medians. They used 1 s time resolution data, collected by a MMP travelling at an average speed 2.7 m s^{-1}. The minimum number of runs needed to obtain representative concentrations was defined as the point at which these mean/median values calculated using a sub-set of runs came within a certain percentage deviation (15%–25%) of their "representative values". They defined the "representative values" as the mean/median of all available runs. Peters et al. (2013) using a 15% deviation percentage concluded that for UFP concentrations the number of runs needed was 16 and 18 for the two sites considered. Van Poppel et al. (2013) used a portion of the data set used in Peters et al. (2013) study and concluded that for UFP concentrations, a 25% deviation could be achieved from 10–16 and 8–16 runs depending on the street, for analysis without and with background correction, respectively.

In a continuation of this work, Van den Bossche et al. (2015) used a large dataset (96–256 runs) of BC measurements for a similar exercise. BC was measured at 1 s time resolution but as discussed earlier, the spatial resolution of these data is variable and complex due to the use of a post-data processing technique (ONA). Allowing replacement in the random selection of runs and employing a background correction, trimmed mean and 25% deviation they concluded that the number of runs needed is 14–61 depending on the street, and also showed that this rose to 108 runs when considering a spatial resolution of 20 m. Prior studies (Peters et al., 2013; Van Poppel et al., 2013) done with small UFP data sets are different from this study in terms of both the way in which the minimum number of required runs is defined and in the spatial scale considered.

Despite these differences, our estimate of the minimum number of runs needed for representative UFP concentration values is also comparable with these two prior studies.

2.4.3 The effect of spatial resolution on the estimate of minimum number of runs needed for representative concentration maps

To investigate the effect of spatial resolution on the estimate of the minimum number of runs needed for representative concentration values we conducted the data experiment described in section 2.4.2 on both HEV spikes removed and HEV spikes retained data sets, using a spatial resolution of 10 m (Fig. 10). For both data sets, the initial values of the maximum relative error are markedly decreased with decreased spatial resolution and the minimum number of runs needed for representative concentration values generally decreases for all the streets and for both AM and PM sessions.

For HEV spikes removed data the maximum relative error along streets also drops from the initial values of 123% - 82 % to 50% in just 3-5 runs (Fig. 10 (a).) The estimate of the minimum number of runs needed for representative concentrations also drops slightly at 10 m spatial resolution, ranges16-18 runs for the mornings and 14-16 runs for the afternoons (Fig. 10 (a)). For HEV spikes retained data the maximum relative error along streets also drops from the initial values of 202-136 % to 50% at 6-12 runs (Fig. 10 (b)) and drops below 15 % only 4 sessions out of the 8 sessions. For all the streets maximum relative error along the streets drop below 17% for 20-23 runs for the mornings and for 18 runs for the afternoons (Fig. 10 (b)). Hence we conclude that the of the minimum number of runs needed for representative concentrations at 10 m spatial resolution is at least 20-23 runs for the mornings and at least 18 runs for the afternoons.

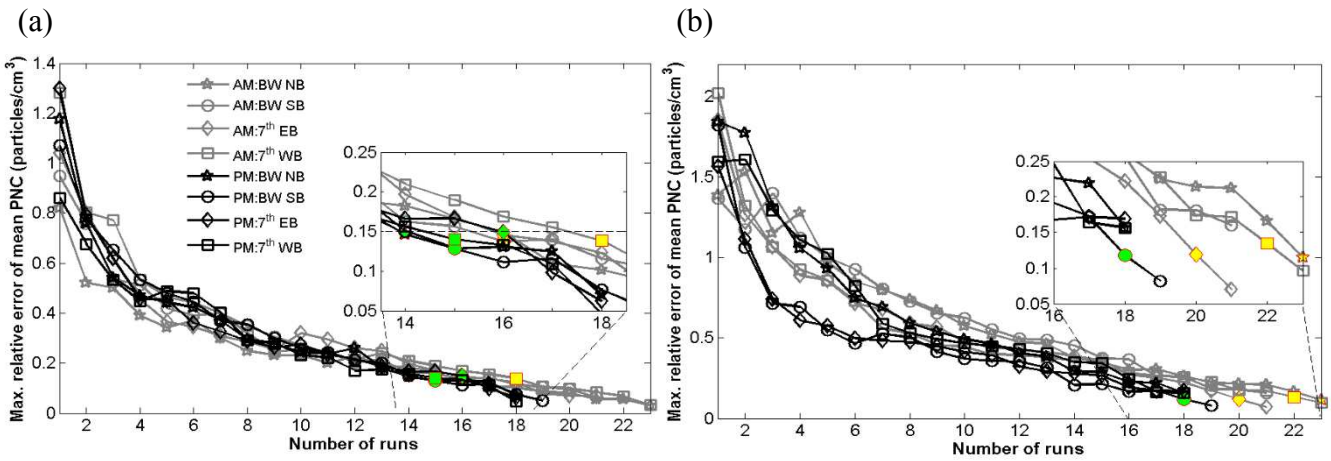

Fig. 10 The variation of maximum relative error along different street segments vs. the number of runs averaged for morning (AM) and afternoon (PM) sessions (a) for HEV spikes removed data and (b) for HEV spikes retained data. The green and yellow symbols denote the points at which the relative error is at or below 0.15. The spatial resolution of the maps considered is 10 m.

3. Effectiveness of vegetation and sound wall-vegetation combination barriers on pollution dispersion from freeways under daytime and early morning conditions

3.1 Introduction

Physical barriers affect pollutant concentrations by increasing turbulence and initial mixing of the emitted pollutants (Hölscher et al., 1993). Roadside solid sound walls (SW), also known as noise barriers, force pollutants to move up and over the barrier, creating the effect of an elevated source and enhancing vertical dispersion of the plume. The dispersion is further enhanced by a highly turbulent shear zone characterized by slow velocities and a recirculation cavity created on the lee side of the barrier. These effects contribute to a well-mixed zone with lower pollutant concentrations downwind behind the barrier (Bowker et al., 2007).

Vegetation barriers have potential to alter flow as well, but with several differences. Vegetation imposes a drag on the air moving through the leaves and branches. This flow obstruction causes some air to move up and around the canopy, thus increasing vertical mixing and in turn reducing pollution concentrations downwind of the barrier. Vegetation can also remove some gaseous pollutants by absorption and particulate matter by deposition (Abhijith et al., 2017 and references therein). The deposition of the smallest particles is controlled by Brownian diffusion, while interception and inertial impaction determine the deposition of larger particles (Petroff et al., 2008). On the other hand, the imposed drag on the airflow creates a windbreak effect behind the vegetation barrier, characterized by lower wind speeds and lower turbulence in the wake of the canopy (Wang et al., 2001). This windbreak effect decreases both dispersion and the rate at which traffic-related pollutants can be advectively transported away, potentially increasing

the pollutant concentrations downwind of the barrier.

While general features of pollutant concentrations downwind of barriers are emerging, concentrations downwind of specific barriers can vary widely depending on many factors. For solid sound walls, the dominant features include the physical characteristics of the barrier such as the height, length, distance from road, number of barriers and their orientation with respect to the wind (Hagler et al., 2011; Heist et al., 2009), meteorological conditions such as wind speed, wind direction and atmospheric stability (Baldauf et al., 2008; Finn et al., 2010), traffic activity such as vehicle volume, speed and fleet mix (Baldauf et al., 2008), and configuration of the road such as the elevation/depression relative to the terrain (Heist et al., 2009) and surrounding structures/vegetation (Bowker et al., 2007). The impact of vegetation barriers on pollution dispersion can depend on several additional variables, including density of the vegetation, seasonal growth patterns, leaf type (Fujii et al., 2008), leaf area index (LAI)/leaf area density (LAD)/optical porosity (Steffens et al., 2012; Ghasemian et al., 2017) and tree canopy type.

In open street environments, solid sound walls can reduce the UFP concentrations by up to about 50% compared to open road values, within 15-50 m on the lee side of a sound wall (Bowker et al., 2007; Baldauf et al., 2008; Heist et al., 2009; Ning et al., 2010; Finn et al., 2010). Understanding of the effectiveness of combination barriers; sound walls together with vegetation barriers, is very limited and studies are few (Bowker et al., 2007; Baldauf et al., 2008). One field study has showed that a combination barrier can augment the reduction of pollutant concentration compared to sound wall-only values (Baldauf et al., 2008), but the authors acknowledge that the proximity of the measurement transects to the edge of the barrier and wind direction dependencies, might have influenced this result. The impact of vegetation barriers alone on pollution dispersion

is also an open question; studies of this barrier configuration have produced inconsistent findings. While some field work (Hagler et al., 2012; Tong et al., 2015; Morakinyo et al., 2016) showed high variability in the effectiveness of vegetation barriers alone, other studies found reduction of UFP (Steffens et al., 2012; Al-Dabbous et al., 2014; Lin et al., 2016; Lee et al., 2018), $PM_{2.5}$ (Chen et al, 2016), PM_{10} (Chen et al.,2015), BC (Brantley et al., 2014), CO (Lin et al.,2016) and NO_2 (Fantozzi et al., 2015a) behind vegetation barriers. Furthermore, vegetation varies widely with location.

Here we attempt to develop a better understanding of the effectiveness of vegetation usually found in the semi-arid climate of California in reducing the pollution concentrations downwind of roads under different meteorological conditions. We present results from an extensive field measurement campaign to investigate the pollution reduction efficiency of vegetation and sound wall-vegetation combination barriers. Data from mobile and stationary measurements were collected at two sites in California (Santa Monica and Sacramento), each with different barrier configurations. Data were collected during daytime at the Sacramento site and in the early morning at the Santa Monica site, to examine effect of different meteorological conditions on decay profiles.

3.2 Measurements

3.2.1 Pollution and meteorological measurements

Mobile measurements were conducted at two sites in California using the ARB mobile monitoring platform (ARB-MMP), an electric sub-SUV fitted with a suite of instruments that measure several particulate and gas phase pollutants (Table 4). The ARB-MMP inlet design and

calibration procedures are provided elsewhere (Hu et al., 2009; Choi et al., 2012) and thus are described only briefly here. For the summer measurement session at the Santa Monica site, a zero-emission electric vehicle equipped with a DiSCmini (Testo) and a GPS unit (Qstar XT) was used as the MMP. At each site, mobile measurements were performed on two transects with different barrier configurations, selected to be as close as possible to perpendicular to a heavily trafficked freeway (Figs. 11 and 12). The MMP was driven 12-14 runs (a run is one pass of the MMP along the full length of the sampling route) on the downwind side on each transect and at least three runs on the upwind side. The downwind runs were conducted in six sets of 4-5 runs, completed by alternating between the two transects. After the completion of a set of runs at both downwind transects, an upwind run was conducted at both upwind locations. While completing each upwind run, the MMP was stopped to collect stationary measurements for 2-5 min at an upwind location 20-25 m from the edge of the freeway.

Additionally, we conducted continuous stationary sampling (6-24 hours/day) at an upwind and a downwind location on each transect. Stationary monitoring included UFP total particle number concentration and size distribution (TSI, SMPS 3080), $PM_{2.5}$ (TSI, Dustrack 8520) and BC mass concentrations (Magee Scientific, AE-33 and AE-42). These measurements are discussed in Lee et al. (2018). Wind speed and direction was measured at each site by a sonic anemometer (10 Hz CSAT3, Campbell Sci. Inc., 21 Hz WindMaster, Gill Instruments Ltd.) that was installed on a rooftop close to measurement transects (indicated in Figs. 11 and 12).

Table 4. Monitoring instruments on the mobile monitoring platform

Instrument	Measurement Parameter	Response time[a] (Inlet to record)	Data time resolution
TSI Portable CPC, Model 3007	UFP count (0.01-1μm)	*4 s*	*1 s*
Testo DiSCmini	UFP count (10-700 nm), mean size	*2 s*	*1 s*
TSI FMPS, Model 3091	UFP size (5.6-560 nm)	*9 s*	*1 s*
TSI OPS, Model 3330[b]	Particle size (0.3-10 μm)	*3 s*	*5 s*
TSI DustTrak, Model 8520[c]	$PM_{2.5}$mass	*5 s*	*1 s*
Teledyne API Model 300E	CO	*21 s*	*1 s*
LI-COR, Model LI-820	CO_2	*7 s*	*1 s*
Teledyne-API Model 200E	NO, NO_2, NO_x	*22 s*	*1 s*
Magee Scientific Aethalometer, AE-33 and AE-42	Black Carbon (BC)	*25 s*	*1 s*
Vaisala Sonic Anemometer and Temperature/ RH sensor	Surface winds, temperature, relative humidity (*RH*)	-	*1 s*
Garmin GPSMAP 76CS and Qstar travel recorder XT	Qstar travel recorder XT	-	*1 s*
Eurotherm Chessell Graphic DAQ Recorder	Data-logger	-	*1 s*

[a] Response time is an averaged value for smoke test results (Choi et al., 2013 (S3))
[b] At Santa Monica site only
[c] At Sacramento site only

The average heights and optical porosities were estimated for vegetation within ± 100 m of the measurement transects at each site (Figs.13-17). Optical porosity of the vegetation is defined as the fraction of pore spaces and gaps in the total area of the tree crown profile. High optical porosity corresponds to low density vegetation and/or large amounts of gaps between trees. The optical porosity of the vegetation barriers was estimated by measuring the optical porosity of each tree crown according to a US Forest Service field guide for vegetation characterization (USFS, 2011). The effective optical porosity of vegetation at a site was calculated by rescaling the mean

optical porosity of the site to maximum height of vegetation at either of sites. Horizontal dimensions of the trees and their heights with respect to the highway road surface were measured in Google Earth Pro. The vegetation characterization and estimation of the mean optical porosity are discussed in detail in section 3.2.2.

Two measurement sites with different barrier configurations were chosen. At the morning site in Santa Monica, CA (34° 1'35.97"N/ 118°27'33.66"W), the I-10 freeway had an east-west orientation. In the mornings, the prevailing winds were mostly northerly, and the sound wall of interest was on the south side of the freeway. Downwind mobile measurements were conducted in the mornings (05:00-07:30) on Dorchester Ave. where a combination (sound wall and vegetation) barrier (CB) was present, and on Granville Ave. where a vegetation-only barrier (VB) was present (Fig. 11). The transects were approximately 840 m long. Upwind measurements were conducted on Dorchester Ave. and Granville Ave., on the north side of the freeway.

Measurements were performed in different seasons, in late summer and early fall 2015 and winter 2016 (Table 5). Only UFP measurements were collected during the late summer session; these were grouped with early fall measurements (summer/fall) because the meteorology during both periods was similar. Relative to ground level, the I-10 freeway is elevated by approximately 6 m at both sites. The height of the sound wall at the CB is approximately 4 m. The vegetation at VB site is considerably denser (lower optical porosity) and somewhat taller than the vegetation at the CB site. The mean height and the effective optical porosity of vegetation is 8 m and 0.53, 6 m and 0.79 at the VB and CB sites, respectively (Table 7). Except for several cypress trees at VB site and a pine at CB site, all species are evergreen broadleaf trees, none drop their leaves in winter.

The daytime site in Sacramento, CA (38°32'7.41"N / 121°28'21.55" W) was along the SR-99 freeway which has a north-south orientation. The daytime prevailing winds were westerly/north-westerly on most days, and the barrier of interest was on the east side of the freeway. Downwind mobile measurements were conducted in the afternoons (Table 5) on 19th Ave. where a sound wall and vegetation combination barrier (CB) was present and on and 9th Ave. where a sound wall (SW) was present (Fig. 12). The transects were approximately 540 m long. Upwind measurements were conducted on 19th Ave. and 9th Ave., on the west side of the freeway. The CA-99 freeway was elevated by approximately 1 m relative to ground level at both sites.

Fig. 11 The mobile sampling route at the I-10 site in Santa Monica, CA (blue lines). The green lines denote the vegetation barriers and the red lines denote the sound walls. Map source: Google Earth.

Table 5. Measurement periods and surface meteorology at the sites

Date	Measurement Period	Mean wind speed (m/s)	Prevailing Wind direction[b]	Perpendicular wind percentage (%)[c]	Parallel wind percentage (%)[c]
Santa Monica Summer[a]					
08/12/15	05:15-07:00	0.44	NNW-NNE	81	14
08/13/15	05:00-06:45	0.35	NE-N	64	29
08/26/15	05:25-06:45	0.34	N	56	29
08/27/15	05:15-07:10	0.23	NNE-NNW	59	21
08/28/15	05:35-07:15	0.24	NNE-N	64	27
Santa Monica Fall					
10/01/15	05:40-07:30	0.33	NE	58	42
10/02/15	05:50-07:20	0.35	E-ENE	23	52
10/06/15	05:25-07:15	0.32	NE-ENE	8	75
10/08/15	05:50-07:40	0.33	N-NE	75	20
10/09/15	05:00-07:10	0.41	N-NE	59	30
Santa Monica Winter					
02/22/16	05:11-07:25	0.54	NE	50	44
02/24/16	04:52-07:12	0.98	NNE	74	26
02/25/16	05:04-07:47	0.68	NNE	70	30
03/08/16	05:26-07:35	2.00	NNW - NE	100	0
03/09/16	05:08-07:07	1.20	NE - N	49	39
Sacramento					
06/20/16	13:15-16:45	1.40	W	70.	30
06/21/16	13:45-16:15	1.48	WNW-NW	26	74
06/22/16	12:22-15:15	1.40	SSW	91	9
06/27/16	14:15-17:00	1.70	WNW	94	6
06/28/16	12:45-15:00	1.48	W	45	55
06/29/16	12:30-15:15	1.42	SW	83	15
06/30/16	12:45-15:30	1.37	WNW	70	30

[a] only UFP measurements
[b] prominent (>20% of the time) wind direction is noted first
[c] Mean of percentage of time each transect was under downwind/parallel wind condition (see text for definition) during full length of the measurement period

Fig. 12 The mobile sampling route at the SR-99 site in Sacramento, CA (blue lines). The green lines denote the vegetation barriers and the red lines denote the sound walls. Map source: Google Earth.

The heights of the solid sound walls at the CB and SW sites were approximately 4 m and 5 m, respectively. The SW site had minimal vegetation in the immediate vicinity of the measurement transect, with few isolated tall (~13 m) trees (Table 7). The CB site had a relatively dense line of trees, consisting of honey locust and Australian pine, with a mean height of 15 m and an effective optical porosity of 0.63 (Table 7).

3.2.2 Vegetation Characterization and Optical Porosity of Vegetation

Optical porosity of vegetation is defined as the fraction of pore spaces and gaps in the total area of the tree crown profile. High porosity corresponds to low density vegetation and/or large

amounts of gaps between trees. The height and optical porosity of the vegetation barriers at the measurement sites were estimated by Prof. Ulrike Seibt and Dr.Wu Sun as described below.

The large tree canopies for each highway section was identified from the satellite imagery of Google Earth Pro software (Figs. 13 and 14). Satellite images used dated from 2016. Each highway section investigated spans 100 m-200 m in both directions from each target transect, which should cover most contributions from vegetation under both parallel and perpendicular wind configurations. Additionally, locations of the tree canopies were validated against Google Street View images seen from the highways and from the local roads. For the Santa Monica sites, the identified tree locations were additionally validated in field visits. There was no any significant misrepresentation of tree objects in Google Earth Pro compared with field observations, indicating the reliability of the geo locational data in Google Earth Pro. Horizontal dimensions of the trees and their heights with respect to the highway road surface, and distances to the local road section where air sampling were conducted, were measured in Google Earth Pro. The tree heights at the Santa Monica sites were validated using trigonometric methods in the field and found that measurements from Google Earth Pro were within 10% accuracy compared with field values.

Optical porosity (also known as foliage transparency in forestry) of the tree crowns were measured according to a field guide for vegetation structure measurements by the US Forest Service (USFS, 2011). The tree crown as seen by the observer is compared with the images of tree crowns with known density values on a standard Crown Density–Foliage Transparency Card to determine the optical porosity. Measurements of the optical porosity values of the canopies at the Santa Monica sites were conducted in the field near the highway sound walls using this USFS method (USFS 2011). For canopies at the Sacramento sites, screenshots were extracted from the

Google Street View at the exact locations on the highway and estimated the optical porosity with the same method. For the Sacramento sites, the Google Street View images were shot in August 2016, which is close to the time when we did air sampling.

(a)

(b)

Fig. 13 Aerial view and locations of trees at the (a) vegetation barrier (Granville) and (b) combination barrier (Dorchester) transects in Santa Monica (Map source: Google Earth).

(a)

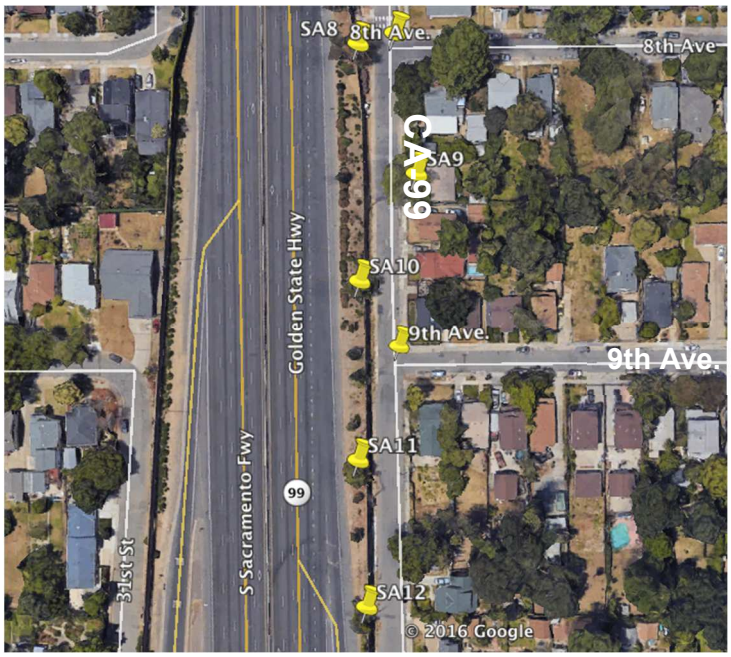

(b)

Fig. 14 Aerial view and locations of trees at the (a) sound wall (9th) and (b) combination barrier (19th) transects in Sacramento (Map source: Google Earth)

The average heights and optical porosity was estimated for vegetation within ± 100 m of the intersection of each transect and the freeways at the Santa Monica and Sacramento sites (Fig.

15 and Fig. 16). Furthermore, an effective optical porosity was calculated of the comparable "scene" for the pairs of transects; this is for a height equal to the tallest tree at either transect. As this calculation includes a significant amount of sky, the optical porosity values calculated this way are quite high. Additionally, the inclusion of trees up to ± 100 m from the transect impacts some of the values; most freeway sections had similar quantities of trees, but the Sacramento 9th street site had a large block of trees beginning ~50m from one end of the transect, so for more perpendicular winds the effective optical porosity will be higher. In general, it is very difficult to link optical porosity directly with tree species, since the leaf area of a tree species is not a consistent parameter, but depends on the tree stand age and environmental parameters such as water stress, nutrient status, etc. With this significant caveat in mind, Table 6 shows a qualitative description of the optical porosity of several species identifiable at the measurement sites.

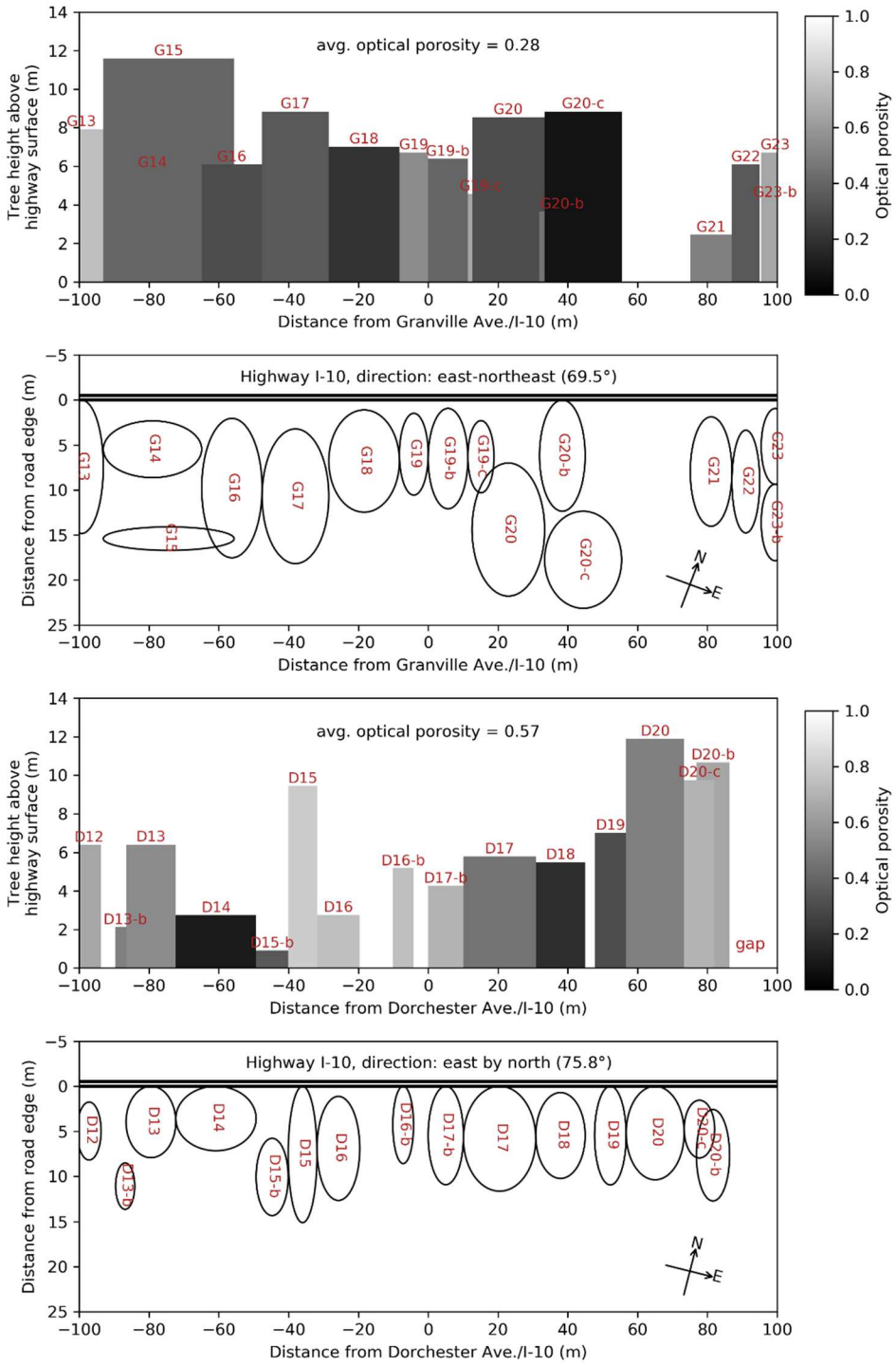

Fig. 15 Profile view (top panels) and top view (bottom panels) of the tree canopies along (a) vegetation barrier (Granville) and (b) combination barrier (Dorchester) transects in Sacramento. In the profile view panels, tree columns are color coded by the optical porosity. The "average optical porosity" indicates the average at the average height of the tree canopy.

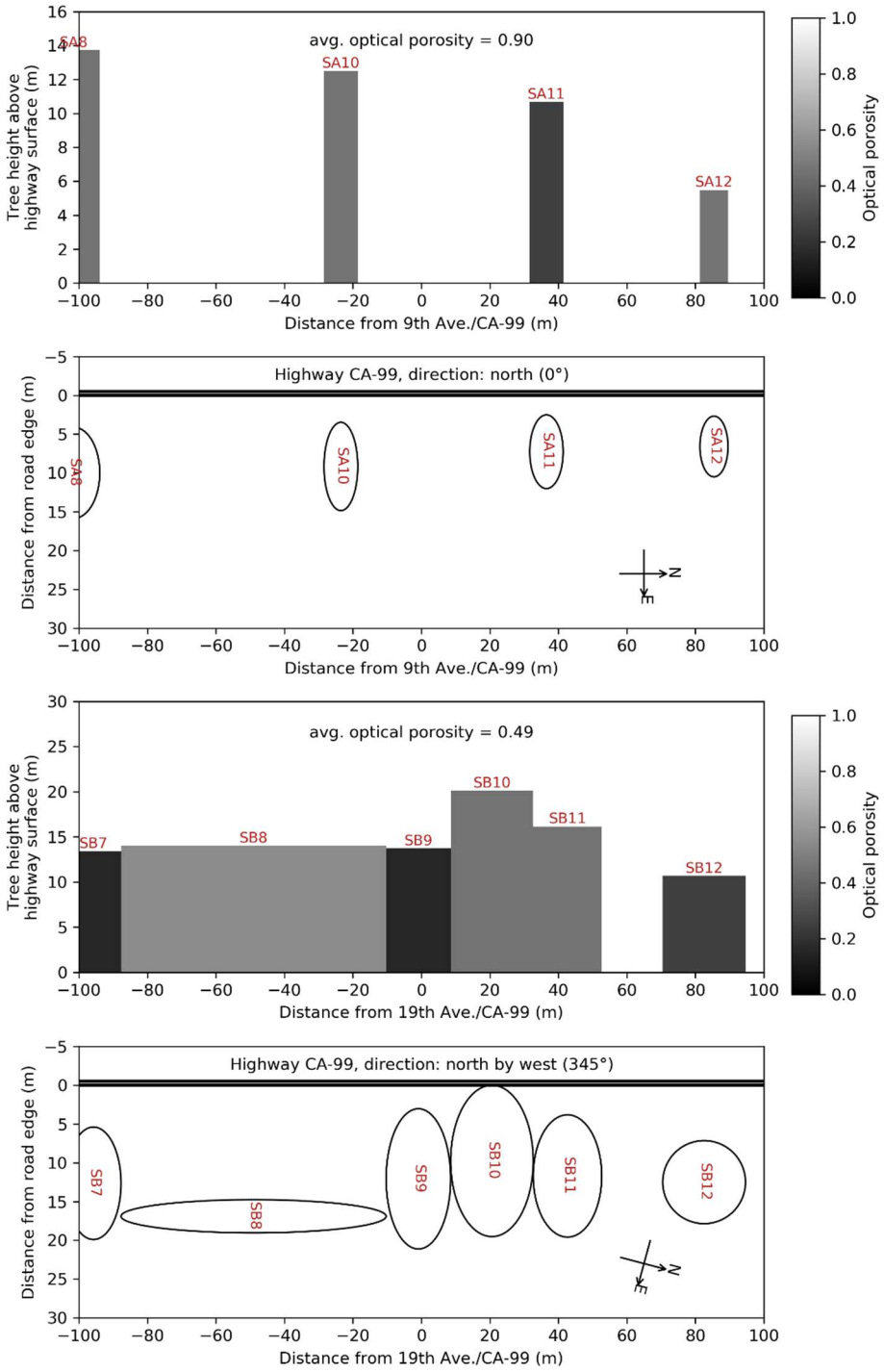

Fig. 16 Profile view (top panels) and top view (bottom panels) of the tree canopies along (a) sound wall (9th) and (b) combination barrier (19th) transects in Sacramento. In the profile view panels, tree columns are color coded by the optical porosity. The "average optical porosity" indicates the average at the average height of the tree canopy.

Table 6. Approximate optical porosity for some representative tree species observed at the study sites in Southern California

Tree species	Optical porosity*
Schinus molle	high
Schinus terebinthifolius	high
Chilopsis linearis	high
Jacaranda mimosifolia	medium
Afrocarpus falcatus	medium
Pinus canariensis	high
Eucalyptus polyanthemos	medium
Cupressus sempervirens	low
Fraxinus uhdei	medium

*High (> 60%), medium (30–60%), low (< 30%). The lower the optical porosity, the denser the tree crown.

Average optical porosity for each section was calculated by weighting optical porosity of individual canopy by length along the highway direction, and height. Gaps between tree canopies were also accounted for by assigning 100% porosity. The average optical porosity was calculated by following the steps below.

1. Calculate the average height of the trees weighted by their widths. If the height of the tree i is h_i, the width is w_i, and the total length of canopy-covered section is W^* (excluding gap segments), then the average height is

$$\bar{h} = \frac{\sum_i h_i w_i}{W^*}$$

Note that gaps between trees are not considered in the above equation.

2. Calculate the height-weighted average crown density using the average tree height $\bar{h}$ as the threshold. For overlapping trees, crown density (δ) in the overlapping cannot exceed one. The

reason to use crown density (1 – optical porosity) for the averaging instead of optical porosity is that, the sky portion above a tree canopy will be automatically accounted as having zero density this way. The average crown density of the section is

$$\bar{\delta} = \frac{\sum_i h_i w_i \cdot \delta_i}{\bar{h} W}$$

where W is the total length of the section including canopies and gaps (200 m).

3. The average optical porosity is then the reverse of the average crown density on a 0 to 1 scale, i.e.,

$$\bar{\theta} = 1 - \bar{\delta}$$

The average heights and porosities for vegetation within ± 100 m of the intersection of each transect and the freeways at the Santa Monica and Sacramento sites are listed in Table 7. Fig. 17 shows the effective optical porosity at each site as a function of height.

Table 7. Average height and average porosity of trees at each location on the primary downwind side, and max height of any vegetation at either of each pair of sites, and the corresponding optical porosity for the max height.

Name	Mean height (m)	Mean optical porosity (dimensionless)	Max height (m)	Mean optical porosity rescaled to max height (dimensionless)
I-10/Granville Ave. (Vegetation only)	7.7	0.28	11.9	0.53
I-10/Dorchester Ave. (combination barrier)	5.9	0.57	11.9	0.79
CA-99/9th Ave. (soundwall only; most vegetation is 50 – 100 m from the center of the	10.5	0.90	20.1	0.95

transect.)				
CA-99/19th Ave. (combination barrier)	14.6	0.49	20.1	0.63

At the Sacramento site, in the immediate vicinity of 9th St. there is minimal vegetation, consisting of a few isolated individual tall (~12 m) trees. As they included in the analysis ± 100 m of the target transect, the scene does show some dense trees, beginning 50 m from the center of the transect.

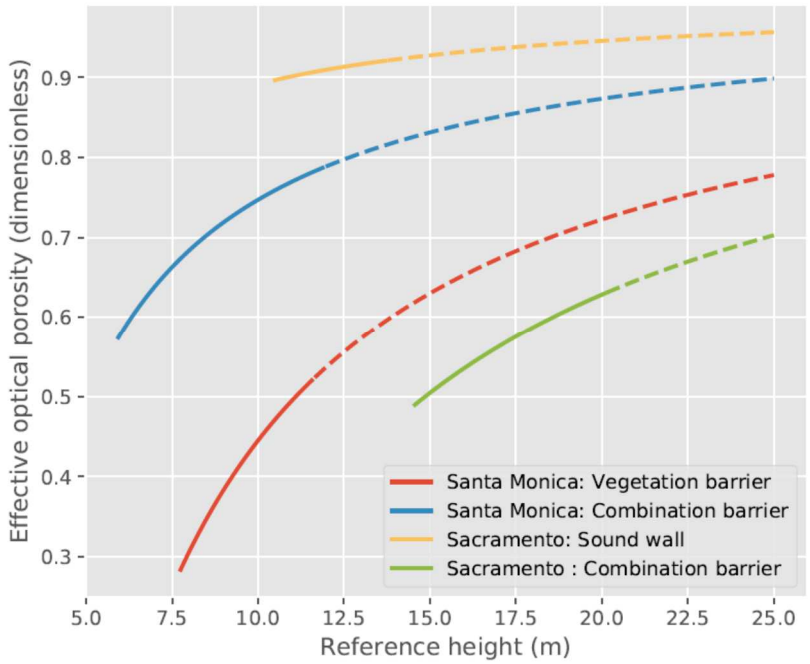

Fig. 17 Effective optical porosity as a function of height. The solid lines indicate the heights up to the maximum height of any tree in the scene; dotted lines include increasing amounts of clear sky. High porosity corresponds to low tree density and/or gaps between trees.

3.3 Data Analysis Methodology

3.3.1 Concentration plots

Deriving accurate concentration profiles from a series of concentration measurements collected on different days and under slightly different conditions requires several steps. Without careful consideration, it is easy to over- or under-weigh some points and/or runs, allow contamination by high-emitting vehicles on the road where sampling was performed to obscure the target source freeway, or include data for runs when the winds were not perpendicular to the freeway. Here we describe the approaches used to handle these limitations. Many of the approaches used here were developed in Ranasinghe et al. (2016) and Choi et al. (2013) and are described only briefly here.

The multi-step process is as follows. First, data from different instruments on the MMP were synchronized to account for the different response times of instruments, using the time-lag correlation method described in detail in Choi et al. (2012). Next, the contribution from high-emitting vehicles (HEV) encountered along the sampling route was removed, by adapting the method developed in Choi et al. (2013) to identify HEV-related spikes. This method uses an iterative statistical approach to establish a site- and session-specific baseline threshold to determine events caused by HEVs, using a specified smoothing time window (60 s) to estimate the baseline.

Close to the freeway, it is more difficult to distinguish the freeway plume from the local traffic emissions. To address this, the threshold value was increased for distances close to the freeway. Site-specific distance bins and threshold values were chosen based on the location of local roads and general traffic volume on those roads during the measurement period. All the

sites were selected such that at close proximity to the freeway, the local roads had minimal traffic, resulting in minimal HEV related spikes. Therefore, all data collected within the first 40 m from the edge of the freeway were retained, and short-lived spikes observed in the time series were manually removed by identifying HEV related incidents using traffic video from the MMP. With increasing distance from the freeway, sites had heavily trafficked arterial road. Hence, the thresholds were exponentially increased as follows. At the Santa Monica site, for 40-150 m, 150-300 m, 300-450 m and > 450 m, the threshold was set to 12, 9, 6 and 3 baseline thresholds, respectively. At the Sacramento site, for 40-75 m, 75-120 m, 120-160 m and > 160 m, the threshold was 24, 12, 6 and 3 baseline thresholds, respectively. All concentration values above the calculated threshold were replaced by the baseline concentration values to obtain the HEV spike-removed concentration time series.

The usage of a site- and session-specific baseline threshold together with distance based cutoff threshold successfully removed the short-lived HEV related spikes, while retaining the slow varying freeway signal (Fig. 18). The HEV removal calculations were repeated with several small increments and decrements to the distance bins and threshold values to investigate the sensitivity of the results to the values chosen in the HEV removal process. No changes were observable in the results, indicating a low sensitivity.

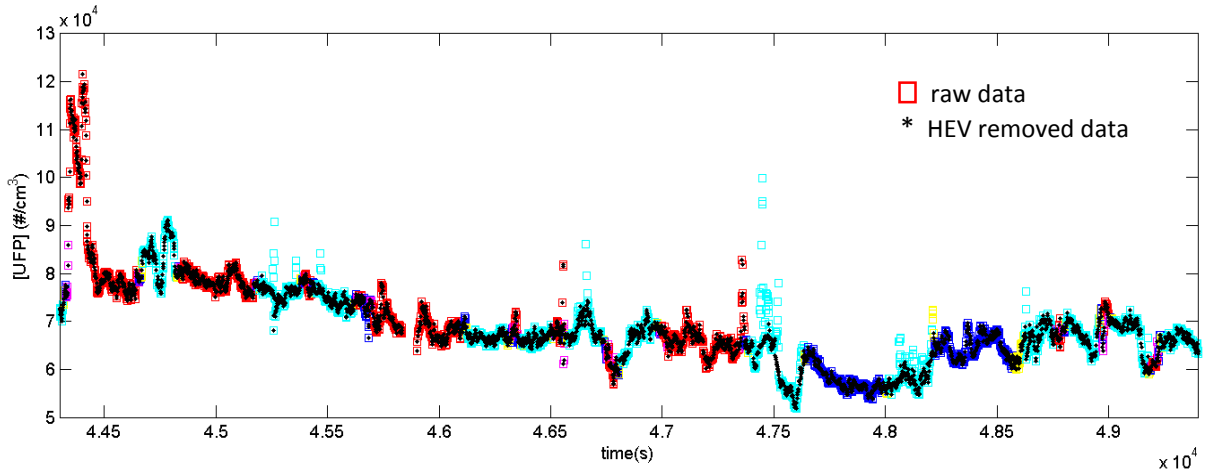

Fig. 18 A HEV spiked removed UFP concentration time series of the Sacramento site. The squares show the raw UFP measurements. Each color represent a bin of distance from the freeway;< 40 m (red), 40-75 m (magenta), 75-120 m (blue), 120-160 m (yellow) and > 160 m (cyan). The squares with black dots show the concentration time series after HEV spike removal.

The effect of barriers on pollution dispersion downwind of freeways has shown to be strongly dependent on the wind direction (Finn et al., 2010, Steffens et al., 2012). We used the meteorological data collected at an upwind location to partition all concentration data according to wind direction. The concentration data were divided into a near-perpendicular data set and a near-parallel data set, defined as wind coming from $\pm 45^0$ from perpendicular or $\pm 45^0$ from the parallel to the freeway, respectively. Next, all the concentration data sets were normalized by the freeway traffic flow at each site; this normalization is described below (Section 3.3.2). As the concentration measurement at a particular time and distance from the freeway is influenced by the emissions and the wind direction from several minutes earlier, we introduced a 10 min lag in traffic flow normalization and wind direction selection, based on the average travel time of pollutants from source to the transects. At each data point, the average traffic flow and wind direction from 10 min earlier was calculated and used for the traffic flow normalization and wind filter.

Next, we used the line reference system developed by Ranasinghe et al. (2016) to provide a framework to organize the data and produce concentration maps at specific spatial resolutions. With this procedure, the GPS data for each run (one pass of the MMP along the sampling route) was used to assign each concentration data point to the closest line reference point along a particular street. Then for each session, all data values assigned to a reference point were averaged, and the standard deviation of the mean calculated. There is a higher data density at the ends of the transects because the MMP was slowed to turn around, and the concentration changes most rapidly near the freeway. To exploit this higher data density at the start of the transect, we used a 10 m spatial resolution in the first 30 m and 20 m spatial resolution thereafter. The number of data points averaged at a line reference point ranged 31 ± 17. For $PM_{2.5}$ and PM_{10} profiles, we used a 40 m spatial resolution because data collected using the OPS (TSI OPS3330) had lower time resolution (5 s) (Table 4).

From day to day, average pollution concentrations vary by a factor of two or more, due to meteorological phenomena such as mixing height, turbulence intensity and atmospheric stability. These variations in the urban background must be accounted for prior to averaging data from different sessions and days to avoid over/under weighting.

In this study, the upwind background stationary measurements were made at 15 m and 10 m from the edge of the freeway in Santa Monica and Sacramento, respectively; upwind mobile measurements were made at 20-150 m from the edge of the freeway at both sites. However, data from these measurements were not used for several reasons; Santa Monica upwind measurements were likely too close to freeway; Choi et al. (2012) showed some influence from the freeway up to 500 m during early mornings, and both Santa Monica and Sacramento sites were influenced by variable winds making the upwind site downwind intermittently. The number

of mobile measurement runs conducted on the upwind side of the freeway was limited to two, due to the limitations on measurement time and mobile platform mileage. The session mean pollution concentration levels of some pollutants on upwind of the freeway are shown below for each transect, when winds were perpendicular to the freeway (Fig. 19). The measurements that were made approximately 15-80 m from edge of the road was extracted.

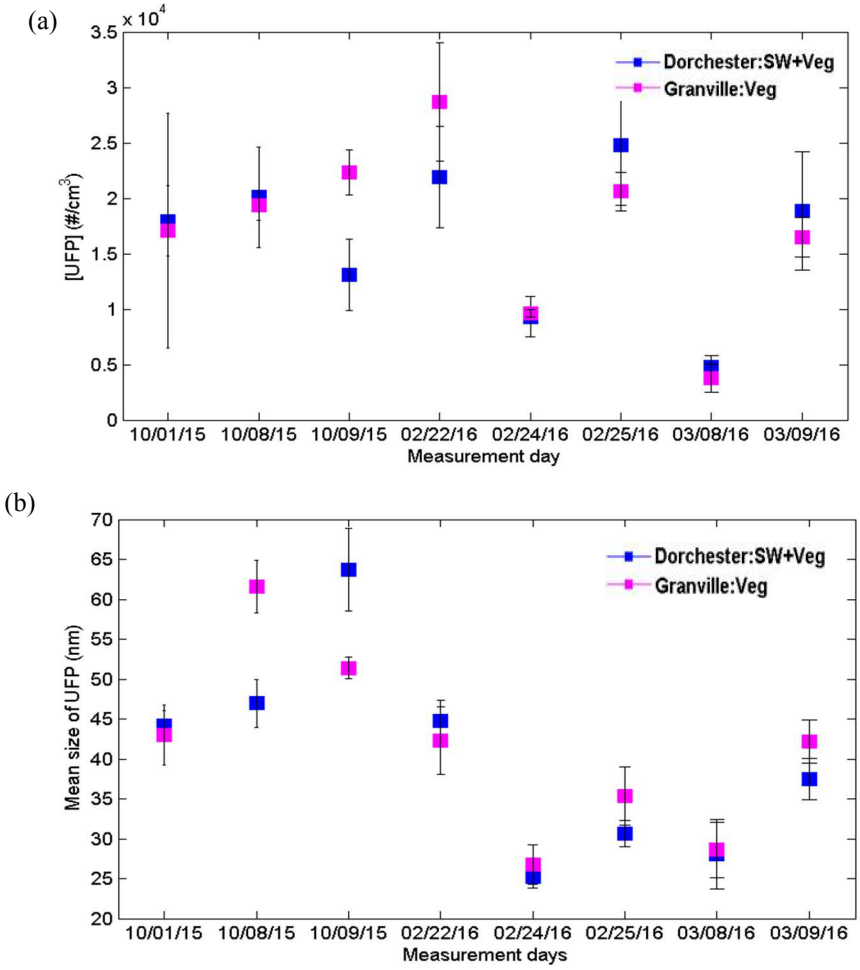

Fig. 19 The upwind (a) number concentration and (b) mean size of UFP along the two transects at the I-10 Santa Monica site, under perpendicular wind conditions for fall 2015 and winter 2016 measurement session. The session mean concentration is plotted together with the standard deviation.

The upwind site characteristics were different for the two transects. In Santa Monica, the Dorchester street upwind site was situated in a low trafficked residential area while the Grandville street upwind site was downwind of busy arterial road. However, on most days the mean concentration levels at upwind sites were similar, whenever sufficiently large data sets were available for both sites (Fig. 19).

To account for the daily variations in the urban background, we normalized the concentration profiles by the daily maximum concentration. The daily maximum concentration of transects was obtained from daily average concentration profiles made from HEV-removed, wind filtered data averaged at line reference points. Then the daily average concentration profiles of both transects were normalized by dividing all values by the daily maximum concentration.

Each day had a different number of data points corresponding to the percentage of time each transect was downwind and had near-perpendicular winds during the measurement period. Moreover, consistent winds give higher quality data with a clearer freeway plume decay pattern. Therefore, we used a weighting factor based on the mean percentage of time transects were downwind on each day. If the mean percentage of time the transects was downwind was below 25%, that day was not included in the averaging. Then the weighted, normalized concentrations were averaged over all days of a session to obtain the general concentration dispersion pattern. The weighted variance over all days of a session was used to calculate the standard error of the mean.

3.3.2 Traffic flow variations

To correct for time and day-dependent variations in traffic, 5 min resolution traffic data was retrieved from the Caltrans Performance Measurement System (PeMS). We chose the

closest main-line sensor on the freeway for each measurement transect and each traffic flow direction, provided that the sensor had > 99% observation rate. The exception was one sensor at the Sacramento site which had a 75% observation rate; there were no better alternatives for this site. All main-line traffic sensors were within 2 km of the transects. When there were on/off-ramps between a selected main-line sensor and the target measurement transect, either measured or historic traffic flow rates from on-ramp/off-ramp sensors were used to estimate the traffic flow at each transect. Traffic data had 5-min time resolution.

Figs. 20 and 21 show the 30 min means of the traffic flow in both directions at each measurement transect, together with the standard deviations of the means. The day-to-day variation in the traffic flows in Santa Monica was small, but slightly different at the two transects; the freeway traffic flow near Granville Ave. was 2.5% and 4.9% higher than the freeway traffic flow near Dorchester Ave. in the fall and winter seasons, respectively. The Sacramento daytime freeway traffic flow varied widely from day to day, and traffic flow near 19th Ave. was 4% higher than the traffic flow near 9th Ave.

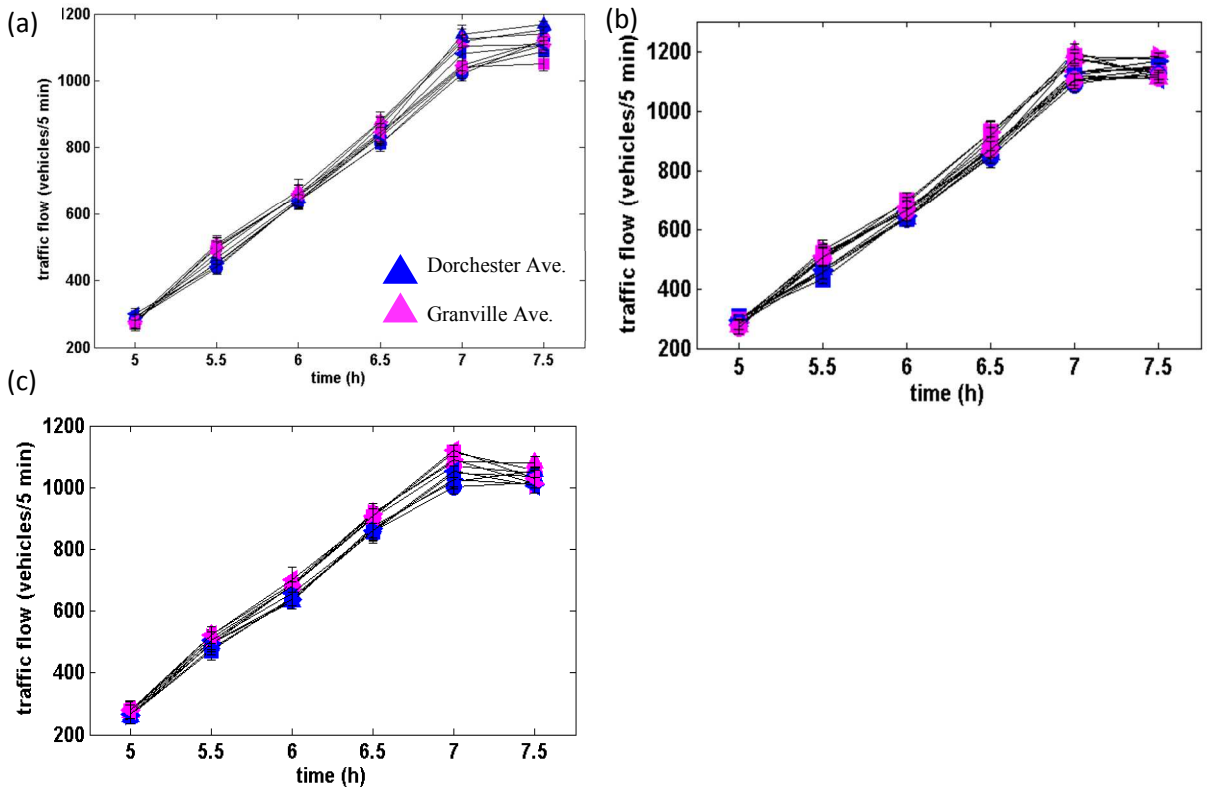

Fig. 20 The diurnal traffic flow variation on I-10 at Santa Monica site, during (a) summer, (b) fall and (c) winter measurement sessions. The 30 min mean of the traffic flow in both directions at each measurement transect (color symbols) and the standard deviation of the mean. Different symbols indicate different measurement days.

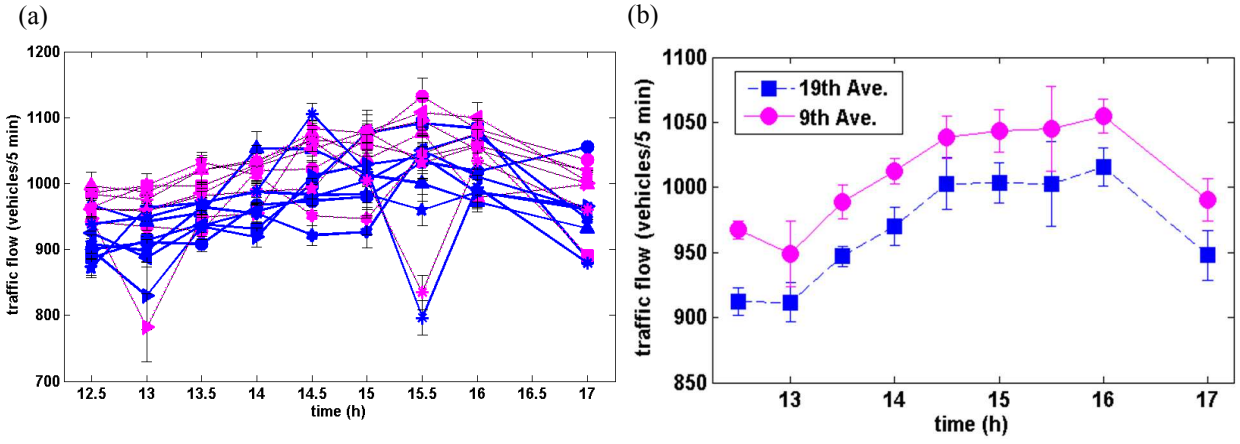

Fig. 21 The diurnal traffic flow variation on SR 99 at Sacramento site. (a) The 30 min mean of the traffic flow in both directions at each measurement transect (color symbols) and the standard deviation of the mean. Different symbols indicate different measurement days. (b)

The 30 min mean of the traffic flow in both directions, averaged of all measurement days, and the standard deviation of the mean.

3.4 Results and Discussion

3.4.1 Combination barrier vs. vegetation barrier

Fig. 22 shows the traffic-normalized ultrafine particle number concentration [UFP] average decay profile under perpendicular wind conditions, for early morning stable atmospheric conditions at the Santa Monica site. In agreement with the earlier studies (Hu et al., 2009; Choi et al., 2012; Choi et al., 2014), the [UFP] gradually decreases throughout the full length of the transect (840 m) in both sessions.

The [UFP] reduction behind the barriers showed different trends in the summer/fall and winter measurement sessions. Under perpendicular wind conditions, in the summer/fall session, the vegetation-only barrier was more effective in reducing downwind [UFP] than the combination barrier (Fig. 22a), while in the winter session, the combination barrier was more effective than the vegetation-only barrier (Fig. 22b). In the summer/fall season, the traffic-normalized [UFP] downwind of the vegetation-only barrier during perpendicular winds was 32% lower than the combination barrier (Fig. 22a), averaged over the entire transect (800 m). Averaged over the first 160 m (~ 525 ft.), this difference was 37%. For the winter season, the traffic-normalized [UFP] downwind of the combination barrier during perpendicular winds was 6% lower than the vegetation-only barrier (Fig. 22b) averaged over the entire transect. Averaged over the first 160 m from the edge of the freeway, this difference was 16%.

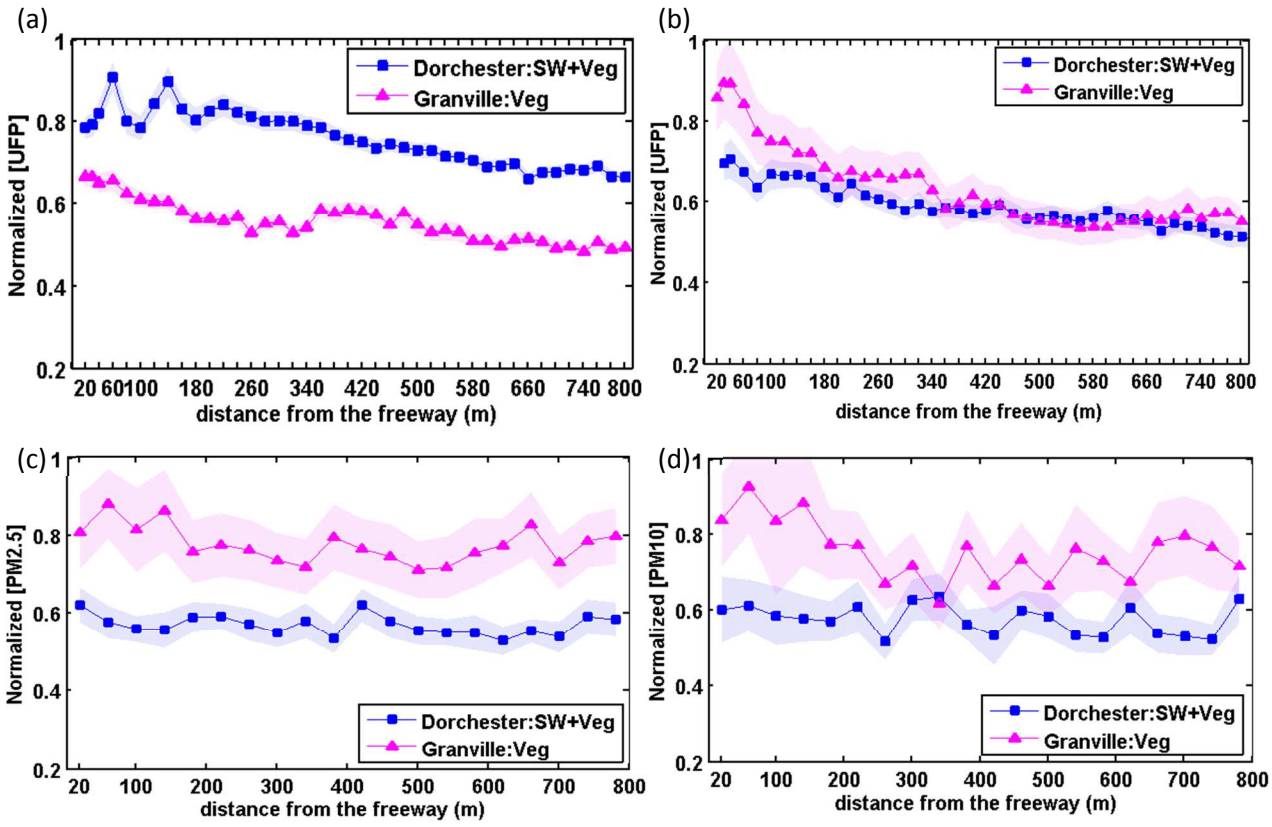

Fig. 22 The normalized (a, b) UFP number concentration and (c) $PM_{2.5}$, (d) PM_{10} mass concentration along the two transects at the I-10 Santa Monica site under perpendicular wind conditions for (a) summer-fall 2015 and (b, c, d) Winter 2016 measurement sessions. The traffic-normalized concentration averaged over (a) 8 and (b, c, d) 5 sessions (lines) is plotted together with the standard error of the mean (shaded areas).

The surface meteorology in summer/fall vs. winter sessions was different in several respects that likely contributed to the observed differences in pollution plume decay downwind of the freeway. The average wind speed in the summer/fall session was 0.3 ± 0.1 m/s, while in the winter session it was 1.1 ± 0.6 m/s; an investigation of the wind speed dependence of the pollution reduction is presented in section 3.4.3. Also, the wind direction was more variable in the summer/fall session than in winter; the average percent time transects were downwind of the freeway (as defined in section 3.3.1) was 55 ± 22% in the summer/fall session and 69 ± 21% in

the winter session. When variable winds cause intermittent switching of the side that is downwind, the (mostly) upwind pollution levels tend to increase and (mostly) downwind pollutions levels tend to decrease, affecting the downwind concentration decay profile.

The pollution profiles are less influenced by the freeway pollution plume under parallel/near-parallel wind conditions and likely to be more influenced by local sources. The benefit of barriers seem very limited under parallel wind conditions in the morning stable atmosphere. Fig. 23 shows the average traffic-normalized [UFP] decay profiles under parallel wind conditions at the Santa Monica site. Compared to the perpendicular wind case, [UFP] decay profiles under parallel wind conditions showed only small reductions along each transect. After a limited initial decay behind the vegetation barrier, there was no significant difference in the concentrations behind the different barriers. The initial [UFP] reduction behind the combination barrier was 19, 7%, averaged over the first 80, 60 m from the edge of the freeway, in fall and winter, respectively.

$PM_{2.5}$ and PM_{10} mass concentration ([$PM_{2.5}$] and [PM_{10}]) data were not available for the fall season, due to instrument malfunction. In winter, under perpendicular wind conditions, the traffic normalized downwind [$PM_{2.5}$] (Fig. 22c) and [PM10] (Fig. 22d) showed a small and in appearance gradual decay with increasing distance, in the first 200 m from the freeway and the particle concentrations behind the combination barrier was lower compared to the vegetation-only barrier. This gradual decay is due to the fact that freeway is a weak source of these pollutants, compared to their background levels (Karner et al., 2010; Choi et al., 2014). The concentration difference that extends along the full length of the transect indicates the likely contribution from an additional area-wide source of $PM_{2.5}$ and PM_{10}. However, the barrier effect on $PM_{2.5}$ and PM_{10} concentrations is similar to that on UFP; the combination barrier was more

effective in reducing fine/coarse particulate matter than the vegetation-only barrier under winter meteorological conditions.

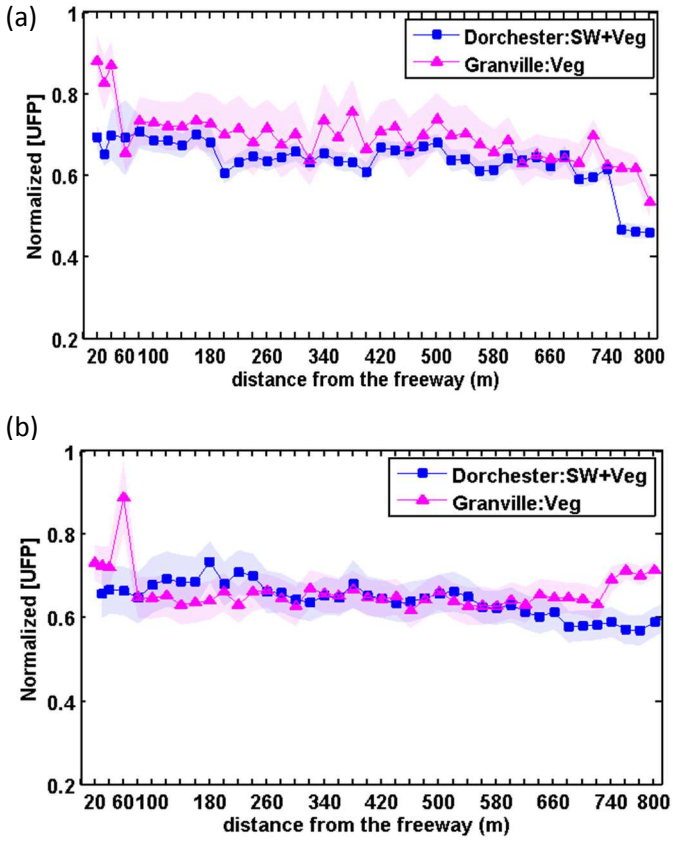

Fig. 23 The normalized UFP number concentration along the two transects at the I-10 Santa Monica site, under parallel wind conditions for (a) summer-fall 2015 and (b) winter2016 measurement sessions. The traffic-normalized concentration averaged over (a) 6, (b) 4 sessions (color plots) is plotted together with the standard error of the mean (shaded area).

Continuous stationary measurements of particulate matter conducted at a site in Encino, CA, a site with a similar barrier configuration (CB and VB); found the same pattern of pollution reduction (Lee et al., 2018). For both [UFP] and [PM2.5], a combination barrier was more effective reducing downwind pollution concentrations under perpendicular wind conditions. The analysis did not distinguish between day and nighttime data. Under perpendicular winds, the

average wind speed was 1.1 ± 0.75 m/s. This indicates that regardless of the atmospheric stability and different site/barrier characteristics, under moderate wind speeds, combination barriers are more effective in reducing downwind UFP and PM2.5 concentrations, than a vegetation barrier alone.

Decay trends of several gas phase pollutants were generally similar to particulate matter pollutants trends. Fig. 24 shows the average traffic-normalized concentration profiles of NO (Fig. 24a, b), NO2 (Fig. 24c, d) and CO (Fig. 24e, f) under perpendicular winds. For all three gas phase pollutants, the reduction downwind of the combination barrier was smaller than the vegetation-only barrier in the fall season (Fig. 24a, c and e); and larger than the vegetation-only barrier in winter (Fig. 24b, d and f). In the fall, under low wind speeds, a gradual decay was observed along the entire transect. In the winter, under higher wind speeds, a relatively steeper decay was observed in the first 100 m from the freeway, followed by a gradual decay along the rest of the transect.

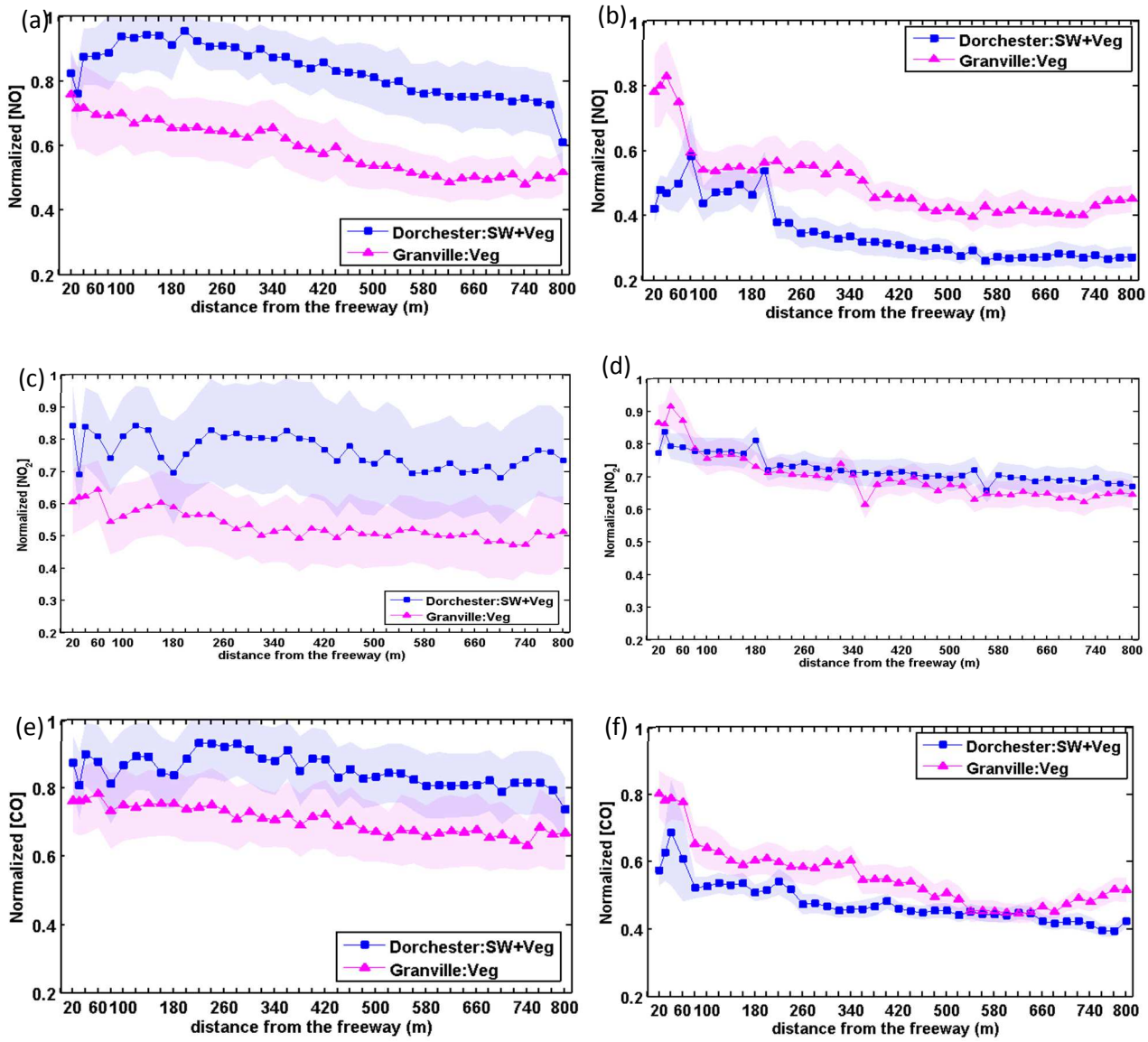

Fig. 24 The normalized (a, b) NO, (c, d) NOx and (e, f) CO concentration along the two transects the I-10 Santa Monica site, under downwind conditions for (a, c, e) Fall 2015 and (b, d, f) Winter 2016 measurement sessions. The traffic-normalized concentration averaged over (a, c, e) 2 and (b, d, f) 5 sessions (lines) is plotted together with the standard error of the mean (shaded areas).

3.4.2 Combination barrier vs. Sound wall

Under daytime unstable atmospheric conditions, elevated pollution levels near freeways decay rapidly (Karner et al., 2010 and references there in). Fig. 25 shows the traffic-normalized

[UFP] and [$PM_{2.5}$] average decay profiles under downwind conditions, in the daytime unstable atmosphere at the Sacramento site. The [UFP] shows a steep decay up to about 160 m from the freeway (Fig. 25a). This is in agreement with numerous studies that have shown near-road [UFP] rapidly returning to background levels within 210-570 m from the freeway (Karner et al., 2010).

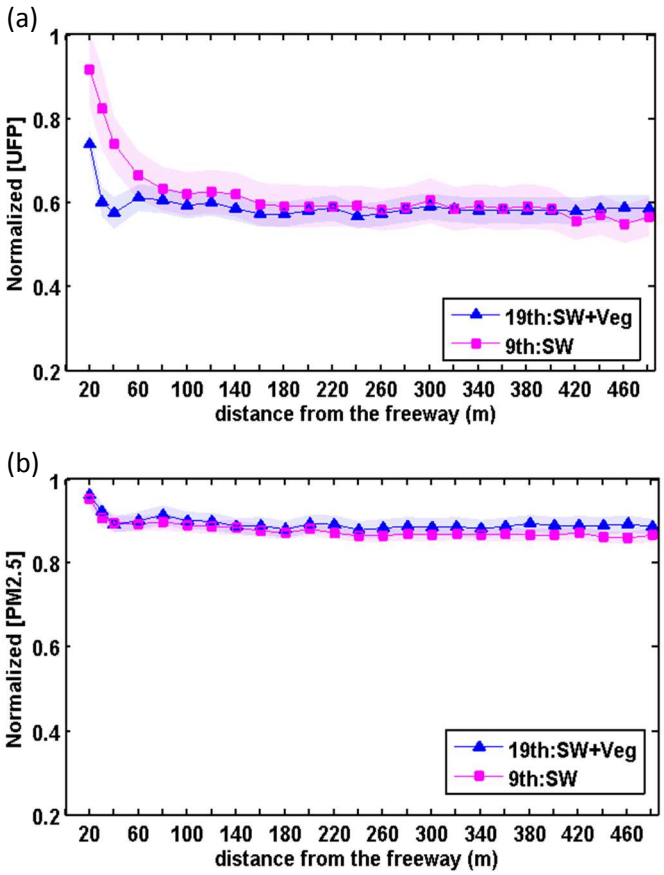

Fig. 25 The normalized (a) UFP number concentration and (b) $PM_{2.5}$ mass concentration along the two transects at the SR-99 Sacramento site, under perpendicular wind conditions. The traffic-normalized concentration from the summer 2016 measurement session averaged over (a) 5 (b) 6 sessions (color plots) is plotted together with the standard error of the mean (shaded area)

Under perpendicular winds, the combination barrier was more effective in reducing downwind [UFP] than the sound wall alone (Fig. 25a). The traffic-normalized [UFP] downwind

of the combination barrier was 11% lower than the sound wall only transect, averaged over the first 160 m (~ 525 ft.) from the edge of the freeway. The vegetation at the Sacramento combination barrier site had a mean height of 15 m and an optical porosity of 0.6; making the effective height of the combination barrier significantly higher than the height of the sound wall at the other transect (~ 5 m). The observed lower pollution concentration behind the combination barrier site, under downwind conditions can be attributed to the increased vertical mixing caused by the tall combination barrier. The pollution reduction difference between barriers was small, but might have been larger had the sound wall at the combination barrier not have been ~1 m shorter than that at the sound wall-only site. This result is in agreement with stationary UFP measurements at this site (Lee et al., 2018) and a previously reported field study that found higher reduction of particulate matter concentration behind a sound wall with surrounding mature vegetation compared to a sound wall only site (Baldauf et al., 2008).

This pollution reduction pattern found here is similar to that of the winter session at the Santa Monica site and stationary measurements a site in Encino, CA (Lee et al., 2018), where the combination barriers were more effective than a vegetation barrier alone. Even though measurements at these three sites were conducted under very different atmospheric stability conditions, the average wind speeds were comparable. The average wind speeds of Santa Monica (winter session), Encino and Sacramento measurement sessions were 1.1 ± 0.6 m/s, 1.1 ± 0.75 m/s and 1.5± 0.1 m/s, respectively. This indicates that regardless of the atmospheric stability and different site/barrier characteristic, under moderate wind speeds, combination barriers are found to be more effective in reducing [UFP] than a sound wall or vegetation barrier alone. The wind speed dependence of the pollution reduction is discussed further in section 3.4.3.

It is important to note that this result is likely limited to vegetation and combination barriers with vegetation densities comparable to the values reported here.

Under parallel wind conditions, there was no elevation of [UFP] close to the freeway and concentrations mostly remain constant throughout the transects, indicating the low influence of the freeway pollution plume (Fig. 26). When averaged over the entire transect, the [UFP] at the sound wall only transect was 14.7% lower than the combination barrier transect. This difference in concentrations could be due the local sources. Similar to the stable-atmosphere case, there seem to be no clear benefit of barriers under parallel wind conditions in daytime atmospheric conditions.

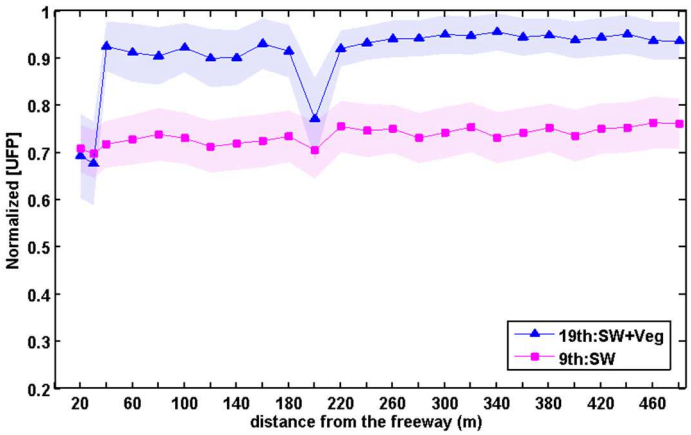

Fig. 26 The normalized UFP number concentration along the two transects at the SR-99 Sacramento site, under parallel wind conditions. The traffic-normalized concentration averaged over 4 sessions (color plots) is plotted together with the standard error of the mean (shaded area)

For [$PM_{2.5}$] (Fig. 25b) the initial decay was very small behind both barriers and there were no differences in pollution concentrations. This may be because [$PM_{2.5}$] near a freeway is only slightly elevated above background, and small concentration differences can be quickly eliminated in rapidly mixing daytime unstable atmosphere.

Profiles for NO_x species generally did show significant differences, consistent with fact that freeways typically have higher NO_x concentrations compared to the background, and thus have a clearer signal. Fig. 27 shows the overall average traffic-normalized NO, NO_2 and CO_2 concentration profiles at the Sacramento site for downwind conditions. The decay trend of the NO and NO_2 was similar to the trend shown by UFP; concentrations behind the combination barrier were lower than behind the sound wall. On both transects, NO and NO_2 decayed rapidly within 20-60 m from the freeway, followed by a slower decay up to 250 m. No decay was observed for CO_2 and the differences in pollution concentrations on the two transects was less than 1%. This is in agreement with previous studies that found CO_2 is not significantly elevated near roads under well-mixed atmospheric conditions (Durant et al., 2010).

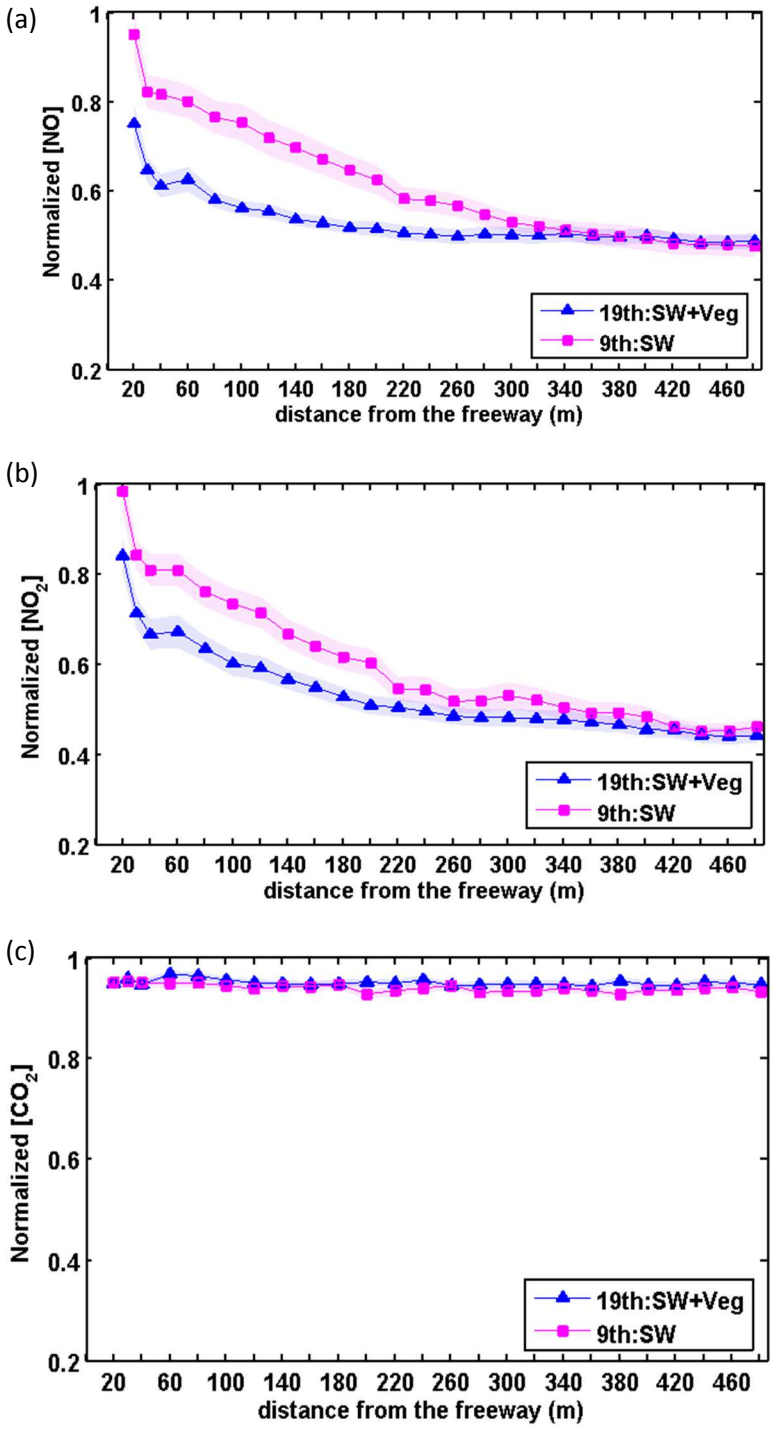

Fig. 27 The normalized (a) NO, (b) NO_x and (c) CO_2 concentration along the two transects at the SR-99 Sacramento site, under downwind conditions. The traffic-normalized concentration from the summer 2016 measurement session is averaged over 5 sessions (color plots) is plotted together with the standard error of the mean (shaded area).

3.4.3 Wind speed dependence of [UFP] pollution reduction

The pollution reduction behind vegetation barriers is attributed to the increasing vertical mixing, and removal of some pollutants via uptake and deposition. The windbreak effect due to the drag imposed on air moving through the porous vegetation barriers has the potential to increase pollution concentrations downwind. Since the porosity, drag force (Kent et al., 2017 and references therein) and particle deposition (Lin and Khlystov, 2012) are wind speed dependent, the pollution concentration reduction by vegetation barriers is expected to be particle size and wind speed dependent. The three measurement sessions at the Santa Monica site had wind speeds ranging from 0.2 to 2.0 m/s, sufficient variation to investigate the wind speed dependence of [UFP] reduction behind the vegetation vs. combination barrier. The range of wind speeds for Sacramento was lower, 1.4 to 1.7 m/s. The relative [UFP] reduction percentage of a combination barrier, in comparison with the vegetation-only barrier (Santa Monica) or a sound wall (Sacramento), was calculated as follows:

For Santa Monica: $$Relative\ reduction = \frac{VEG - CB}{\max(VEG, CB)} \times 100\% \quad \text{(Eq. 5)}$$

For Sacramento: $$Relative\ reduction = \frac{SW - CB}{\max(SW, CB)} \times 100\% \quad \text{(Eq. 6)}$$

Where, CB is the [UFP] behind the combination barrier, VEG is the [UFP] behind the vegetation-only barrier and SW is the [UFP] behind the sound wall. The relative reduction was averaged over the first 160 m from the edge of the freeway and was plotted against wind speed averaged over each measurement day (Fig. 28a and b).

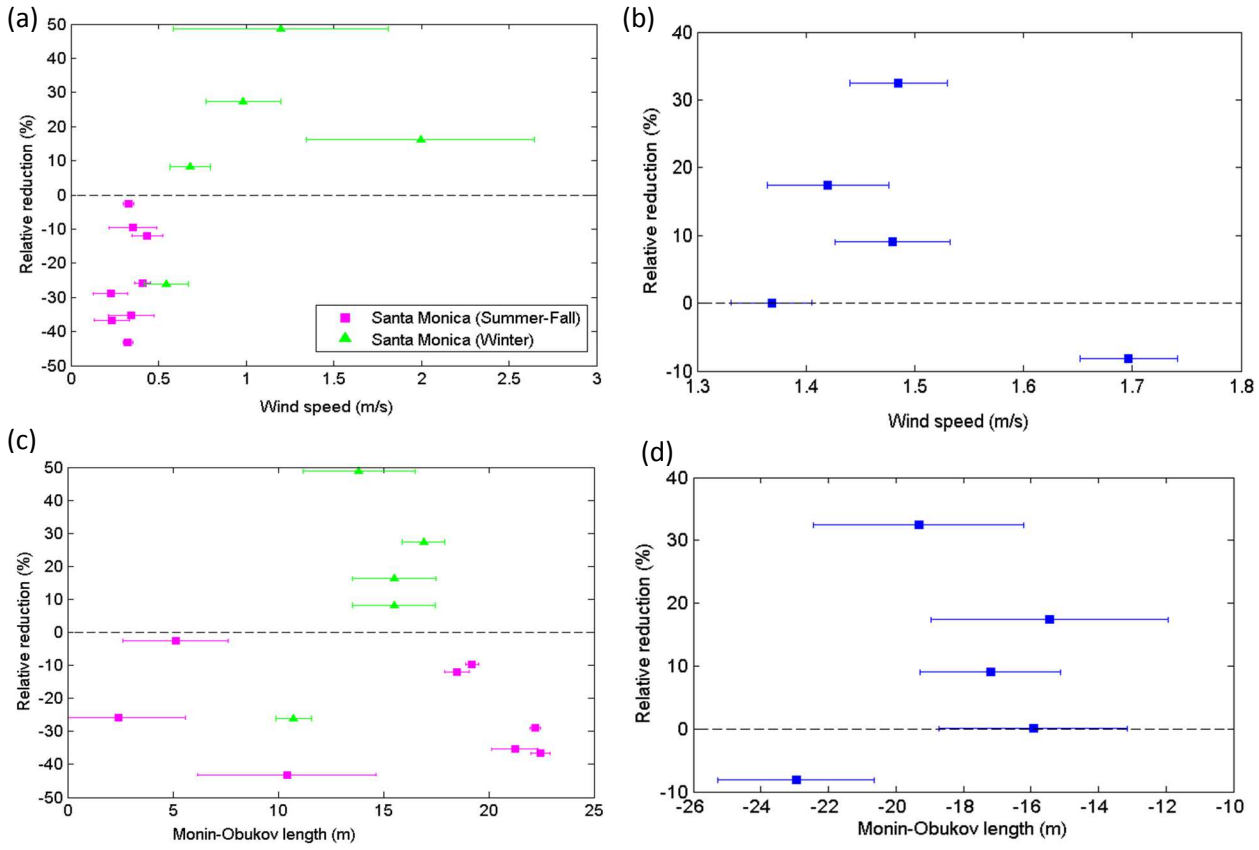

Fig. 28 The relative [UFP] reduction by a combination barrier, under downwind conditions, averaged over the first 160 m from the edge of the freeway for Santa Monica: VEG-CB/VEG (a, c) and Sacramento: SW-CB/SW (b, d) as a function of the wind speed (a, b) and Monin-Obukov length (c, d). Session mean of meteorological parameters are plotted together with the standard error.

Fig. 28a and b shows that the relative reduction in [UFP] is strongly dependent on wind speed. At the Santa Monica site, the vegetation-only barrier is more effective in reducing [UFP] than the combination barrier at very low wind speeds (< 0.6 m/s), indicated by negative relative reduction values, and less effective than the combination barrier at higher wind speeds. Higher wind speeds can increase vegetation porosity, lowering drag force within the vegetation canopy and vertical dispersion, but the difference in vegetation porosity and drag force over the observed

wind speed range is expected be small (Kent et al., 2017). At higher wind speeds the residence time of air mass inside the canopy decreases, resulting in lower molecular diffusion rates and in turn decreasing absorption/depositional removal of pollutants. This dynamic depositional removal efficiency of particles could be the main contributor to the observed wind dependence of the relative reduction. The depositional removal of UFP by vegetation is discussed further in section 3.4.4.

This wind speed dependence of the effectiveness of vegetation barriers in removing UFP is in agreement with a previously reported that used a comprehensive turbulent aerosol dynamics gas chemistry (CTAG) model for vegetation barriers (Steffens et al., 2012) and a wind tunnel that used vegetation branches (Lin and Khlystov, 2012). Lin and Khlystov (2012) reported that the UFP removal efficiency decreased with increasing particle size, increasing wind speed and decreasing packing density (volume fraction occupied by the branches). The sensitivity of removal efficiency to wind speed reported by Steffens et al. (2012) for small particle sizes (< 50 nm) was similar to that found in Lin and Khlystov (2012), but the results diverged for larger particle sizes. Steffens et al. (2012) reported that for particles larger than 50 nm, the UFP removal efficiency increased with increasing wind speed.

This wind dependence can explain the different pollution reduction trends observed at the Santa Monica site in the two different seasons. As above, most of the vegetation at this site consisted of broadleaf trees that maintain their leaf density year around. However, wind speeds differed between the two seasons; all measurement days in the summer/fall session had wind speeds below 0.6 m/s, and 4 out 5 measurement days in the winter session had wind speeds higher than 0.6 m/s (Fig. 28a).

At the Sacramento site, the small number of measurement days and low variability in wind speed makes it difficult to identify a clear trend. Nevertheless, the relative reduction showed a dependence on wind speed (Fig. 28b). At this site, the combination barrier was more effective than the sound wall at wind speeds below 1.5 m/s. The reduction difference between the two barriers seem to decrease at higher wind speeds. Both mobile and stationary data (Lee et al., 2018) from this site indicate that above some threshold value of wind speed (1.5-2 m/s), the sound wall alone could be more effective than a combination barrier. At high wind speeds, while the effectiveness of the mechanisms that reduce pollution concentrations behind vegetation barriers (enhanced vertical mixing and deposition) is reduced, the windbreak effect could be inhibiting free horizontal dispersion of pollutants and resulting in higher concentrations behind the combination barrier compared to the sound wall-only site. Overall, the variations in the relative reduction was smaller for the combination barrier vs. sound wall (Sacramento) than for the combination barrier vs. vegetation-only barrier (Santa Monica) comparison (Fig. 28).

An investigation of the relation between an atmospheric stability (Monin-Obukov length, L) and the relative reduction in [UFP] is presented in Fig. 28c and d. At the Santa Monica site, although all measurement days had very stable atmospheric conditions (small positive L), L was somewhat variable. However, no clear relation was found between the relative reduction and L. At the Sacramento site, all measurement days had moderately unstable conditions (small negative L) and low variability. However, relative reduction generally decreased with increasing L with one exception; the least unstable day that showed higher concentrations behind the combination barrier relative to the sound wall only site. In conclusion, relative reduction has a clearer relation to wind speed than to the atmospheric stability parameter L.

The wind speed dependence of the relative reduction of many pollutants such at $PM_{2.5}$, NO, NO_2 was generally similar to that of UFP, while some pollutants such as PM_{10}, CO showed different patterns (Figs. 29 and 30).

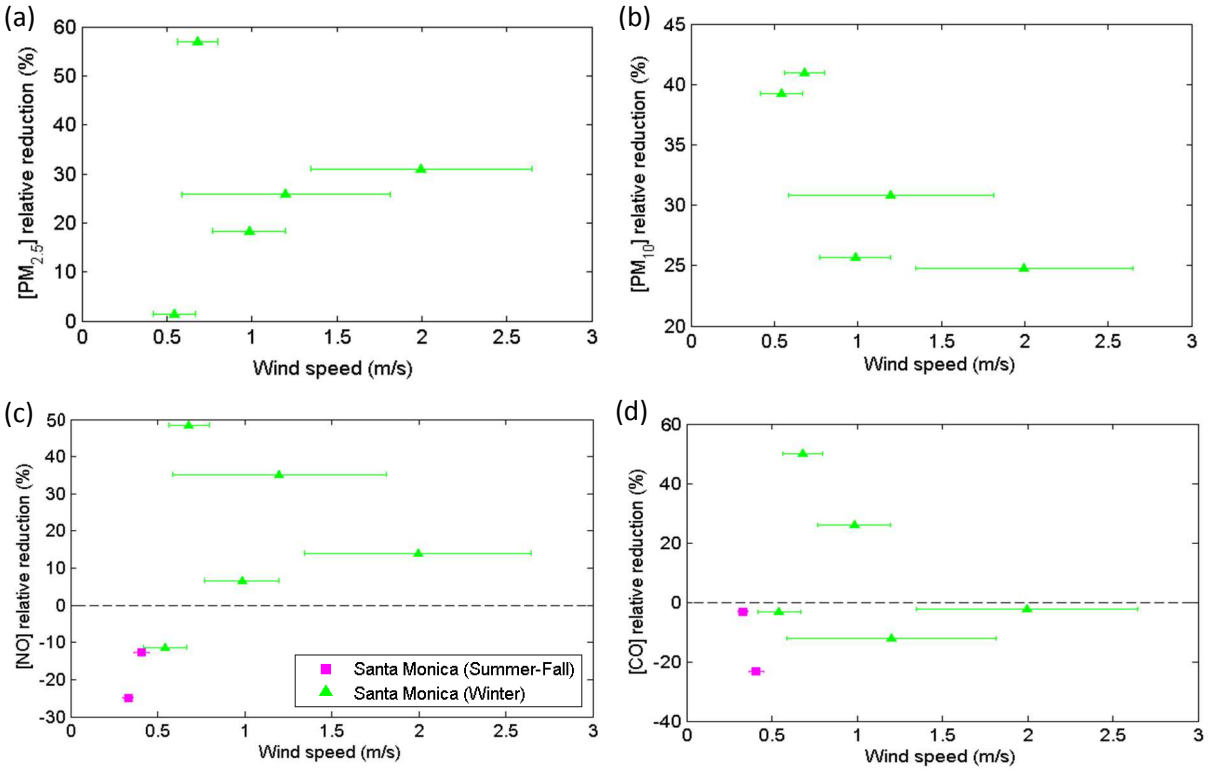

Fig. 29 The relative reduction of (a) $PM_{2.5}$, (b) PM_{10} (c) NO and (d) CO concentrations by a combination barrier, under downwind conditions, averaged over the first 160 m from the edge of the freeway for Santa Monica site, as a function of the wind speed. Session mean of wind speeds are plotted together with the standard error.

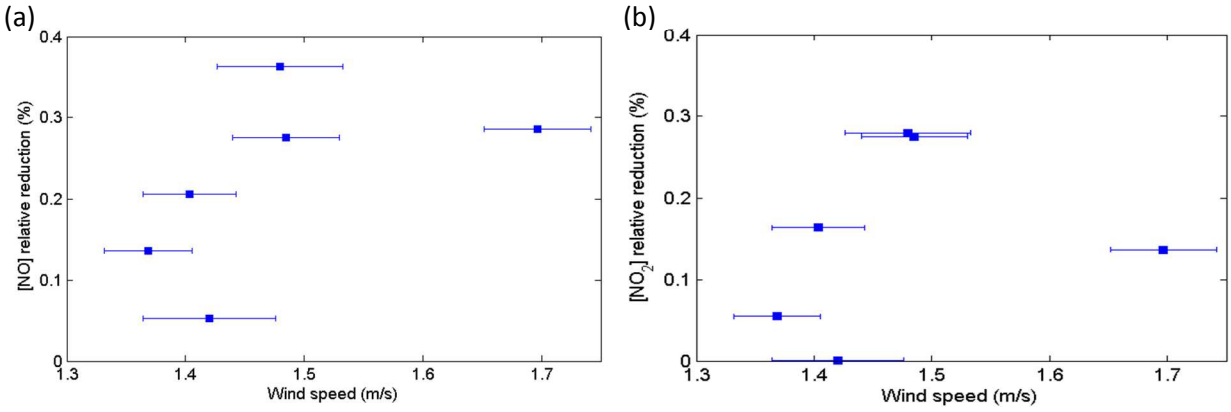

Fig. 30 The relative reduction of (a) NO and (b) NO_2 concentrations by a combination barrier, under downwind conditions, averaged over the first 160 m from the edge of the freeway for Sacramento site, as a function of the wind speed. Session mean of wind speeds are plotted together with the standard error.

3.4.4 Removal of Ultrafine particles by deposition

Roadside vegetation barriers force one part of the freeway plume to move up and over the barrier, while one part flow through the porous barrier. A fraction of the particles in the flow through the vegetation barrier is removed by deposition. The contribution of depositional removal to the particle reduction by vegetation barriers near roadways is a complex function of the characteristics of the vegetation barrier, particles and meteorological parameters. The particle size dependency of deposition could provide insights to the importance of depositional removal in reducing particle concentration downwind of vegetation barriers.

Fig. 31 shows the mean size of UFP downwind of the vegetation-only barrier and combination barrier at the Santa Monica site, in two different seasons. Even though the pollution reduction patterns behind barriers showed a seasonal difference (Fig. 22a and b), the mean size of UFP was larger downwind of the vegetation-only barrier in both seasons. In the first 160m from the barrier, the mean size of UFP was 9% and 5% larger in summer-fall and winter seasons, respectively. This could indicate the contribution of size dependent depositional removal to particle reduction from vegetation barriers.

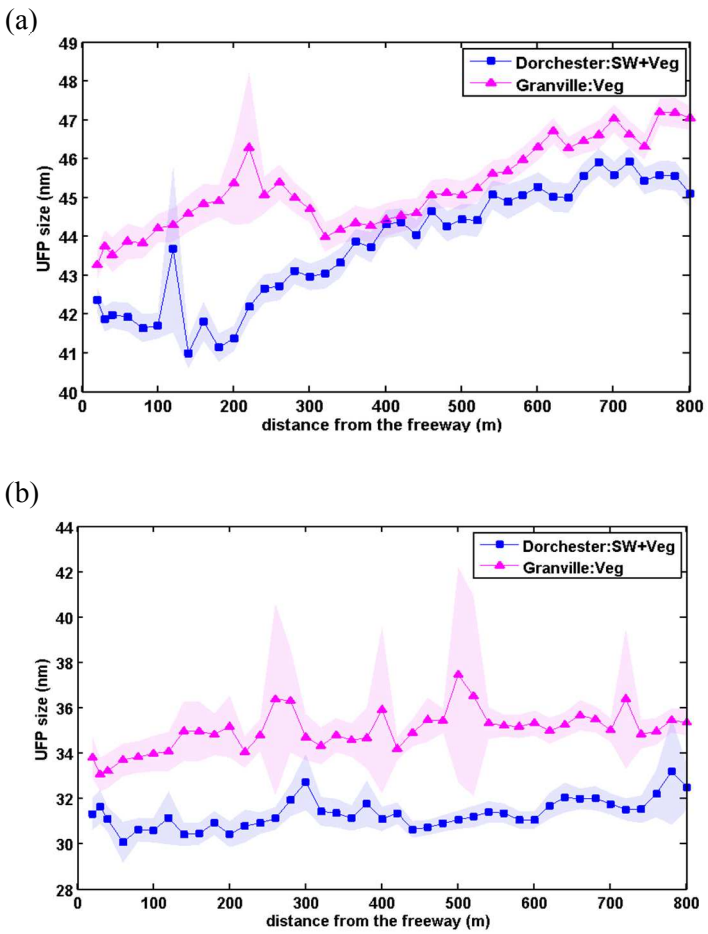

Fig. 31 The mean diameter of UFP downwind of the barriers at Santa Monica in the (a) summer-fall and (b) winter seasons, under downwind conditions.

The increase in vertical mixing created by a solid barrier is larger than that of a vegetation barrier. The background air that is mixed with the freeway plume generally would have larger particles due to atmospheric ageing, in comparison to the freeway plume coming from the source. Therefore, the barrier that creates more vertical mixing would contribute to increase the size of the particles downwind of that barrier. Therefore, when only dispersion is considered, we expect to see larger particle sizes downwind of a solid barrier/combination barrier in comparison to a vegetation barrier. The observed opposite trend in particle size highlights the

contribution of depositional removal in reducing UFP downwind of vegetation barriers, under low/moderate wind speeds and stable atmospheric conditions.

For UFP, diffusion is the dominant mechanism of deposition and the smaller particles with higher deposition velocities are more efficiently removed (Fujii et al., 2008, Lin & Khlystov, 2012). The dispositional removal of particles will contribute to make the mean size of the particles downwind of a vegetation barrier larger. The seasonal difference in the mean size of particles can further indicate the contribution of deposition. The difference in the particle size downwind of the two barriers is much larger in the summer-fall season that had lower average wind speeds (0.3 ± 0.1 m/s) than in the winter season that had higher average wind speeds (1.1 ± 0.6 m/s). The depositional removal of particles is more efficient in lower wind speeds (Fujii et al., 2008, Lin & Khlystov, 2012); so the smaller particles can be more efficiently removed by deposition at lower wind speeds.

The windbreak effect of vegetation barriers reduce the flow velocity and inside and downwind of the canopy. This increases residence time particles in the flow through the vegetation barrier, allowing more time for coagulation, and that would contribute to increase the mean size of the particles downwind. However, the timescale for deposition is approximately an order of magnitude larger than for coagulation, and therefore coagulation is estimated to be not an important process in the neighborhood scale (Kumar et al., 2011 and references therein).

4. Modeling pollution dispersion in near-road environments

4.1 Introduction

Modeling pollutant transport in complex urban areas is a useful tool, but it has many challenges. Dispersion models with a wide range of turbulence characterization complexities have been employed to quantify and predict pollution concentrations, with varying success. They can be loosely categorized into parameterized dispersion models, semi-empirical operational models, chemistry-transport models and computational fluid dynamics models (CFD) (Reynolds averaged Navir Stokes (RANS) /Large-Eddy Simulations (LES)).

Two types of widely used models at the opposite ends of complexity are dispersion and computational fluid dynamics (CFD) models. Dispersion models require parameterization of dispersion coefficients, which are determined by several meteorological factors. However, the detailed turbulence information is affected by surrounding built-environments and quantified relationships between them are unresolved in dispersion models. Nonetheless, dispersion models are cost-effective in computing power and time. On the other hand, CFD models explicitly solve the flow fields through complex built environments by explicitly solving the Reynolds-averaged Navier-Stokes equations. When coupled to a mass transport model they can produce concentration fields of interest. Despite their explicit solutions, CFD models are intensive consumers of computational power and time. The high costs limit the amount of different building morphologies, meteorological and traffic variations that can be tested, making them difficult to use with a large data set with multiple variables.

A modeling environment that can be effectively used with a large data set with multiple sites and multiple variables is a modified dispersion model referred to as the "Quick Urban &

Industrial Complex" (QUIC) (Brown et al., 2010). QUIC is an empirically based, fast-response model with computing time of minutes to hours. It achieves this computational efficiency by parameterizing the flow field around obstacles rather than directly solving the governing momentum equations. Unlike conventional dispersion models, QUIC can incorporate specific building geometries to account for the effects of the built environment on dispersion patterns, include vegetative canopies and moving point sources, all of which improve the capability of determining the influence of the many factors controlling block and sub-block level variations in air pollutant concentrations in urban environments. Furthermore, the QUIC model has multiple particle size handling and indoor infiltration and population exposure calculations, making it a potentially useful tool in urban air quality studies. Despite the promising capabilities of the QUIC model in investigating the traffic related pollution dispersion in urban environments, it had only been used few times in conjunction with field measurements (Zwack et al., 2011; Fernando et al., 2010; Bowker et al., 2007). In each of these instances good agreement was found between the model outputs and field observations and QUIC was found to capture the modification of flow around obstacles well.

QUIC consists of two main model components; a wind solver (QUIC-URB) and a dispersion model (QUIC-PLUME). QUIC-URB is a mass-conserving, empirically based diagnostic three-dimensional wind-field model that simulates fine-scale wind field around obstacles (Röckle scheme) (Pardyjak & Brown, 2007). The flow field within the entire domain is initialized using a logrithmic velocity profile. Based on an incident flow and empirical parameterization of flow effects around objects, an initial uniform wind field is prescribed. This initial wind field is specified as a unidirectional reverse flow. After the initial wind field is forced to be mass consistent, recirculation flows develop in areas where separation and/or low-pressure

regions occur and the analyzed wind field is obtained. These reverse flow regions act as a "fix" for a mass consistent flow model that does not include the momentum equations.

QUIC-PLUME is a Lagrangian random walk model. The mean wind fields calculated by the wind solver are linked to this to produces the turbulent dispersion of pollutants using additional drift terms computed. The normal and shear stresses and turbulent dissipation is determined based on similarity theory, gradient transport and a non-local mixing formulation that approximate the turbulent mixing in building cavities and street canyons (Brown et al., 2010). Usage of several line sources to simulate the tail-pipe release of the traffic, accounts for the vehicle-induced turbulence.

4.2 Model setup

The QUIC (version 4.3, Los Alamos National Laboratory/University of Utah) simulations were conducted for two sites near I-10 Santa Monica, where field measurements of pollutant concentrations and surface meteorology data were available for two seasons (described in section 3.2.1). Each site was simulated separately with a model domain of 700 m in the along-wind direction, 1200 m in the crosswind direction and 50 m in height. The model resolution was set to 2 m×2 m×0.5 m. The model domain consisted of one city block of buildings and barriers on the upwind side of the freeway and several city blocks on the downwind side. Buildings and solid barriers were represented using solid, non-permeable blocks. The specific shapes of the building were extracted using GIS shape files (ArcMap 10.5). The locations and dimensions of all barriers were extracted from Google earth imagery.

Vegetation barriers were represented using permeable blocks with a specified attenuation coefficient. The only vegetation canopy characteristic available from field measurement was the

optical porosity. In both sites in Santa Monica, the vegetation barriers had moderate optical porosities. Due the complex nature of vegetation canopies, there was no direct method available to convert optical porosity values to attenuation coefficients. The attenuation coefficients of vegetation is species dependent and are estimated to be ~1 for coniferous canopies (Cionco, 1978). For the Granville site that had a vegetation-only barrier, several simulation were conducted with different attenuation coefficients. The concentration profiles downwind of the barrier showed low sensitivity to changes in the attenuation coefficient with increasing distance from the barrier (Fig. 32). We choose a constant attenuation coefficient of 1 for all vegetation barriers, in all barrier inter-comparison tests.

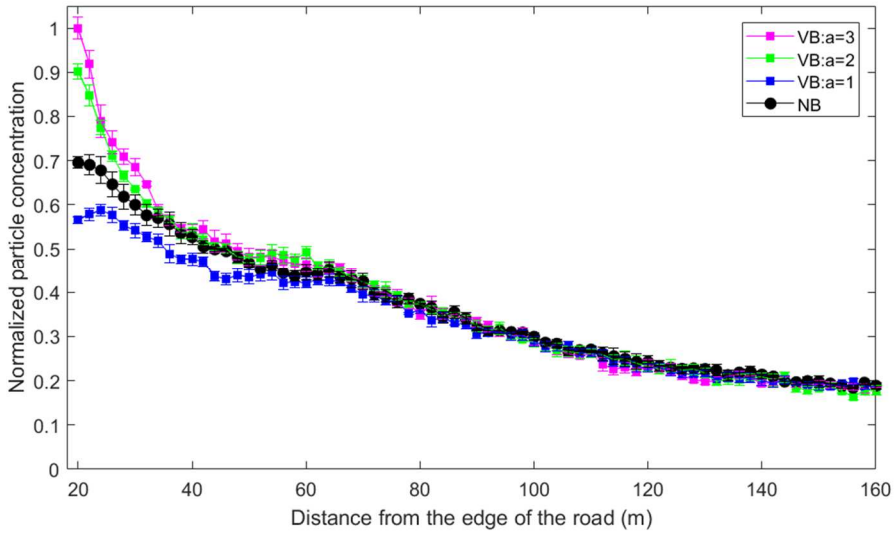

Fig. 32 QUIC model simulated particle concentrations downwind of a vegetation-only barrier, for different attenuation coefficients (a) of the vegetation. The wind speed at the reference height is 1.1 m/s and wind direction is perpendicular to the barrier. The mean concentration (symbol) is plotted together with the standard error (whiskers). The model run with no barriers (NB) is also shown.

Many of the QUIC-URB simulation inputs were derived from the meteorological data gathered at the field measurement sites. Session mean values of wind speed (0.35 m/s and 1.1 m/s at a 5.7 m reference height) and Monin-Obukov length (13.3 m) were used. The input wind direction was kept exactly perpendicular to the freeway. The model domains consisted of low built areas with mostly 1-2 story houses with heights around 5 m. Therefore, the roughness length was set to ~10 % of the urban canopy height, at 0.5 m.

Representing the tail-pipe emissions from traffic flow, two line sources that were parallel to the barriers continuously released particles at a height of 1 m. There was no deposition model available for vegetation barriers. Therefore, particles undergo diffusion and dispersion based on the velocity fields calculated by QUIC-URB. The model was run for 600 s to reach equilibrium state before collecting particle to produce time average concentrations. The total run time of the model was 3000 s and concentration at each grid point was calculated every 1200 s.

4.3 Results and discussion

The QUIC simulated concentration fields for the two sites (Fig. 33) showed complex spatial gradients in both along-wind and cross-wind directions, due to the influence of the barriers and surrounding buildings on the surface level winds. The cross-wind concentration gradients show that the pollution concentration at a particular downwind distance along a field measurement transect (dash lines in Fig. 33) may be not representative of the pollution exposure at a particular house, at the same downwind distance. This highlights the importance of cross-wind field measurements for accurate assessments of concentration gradients, and shows the potential of built-environment resolved model simulations to improve exposure assessments in near-road communities.

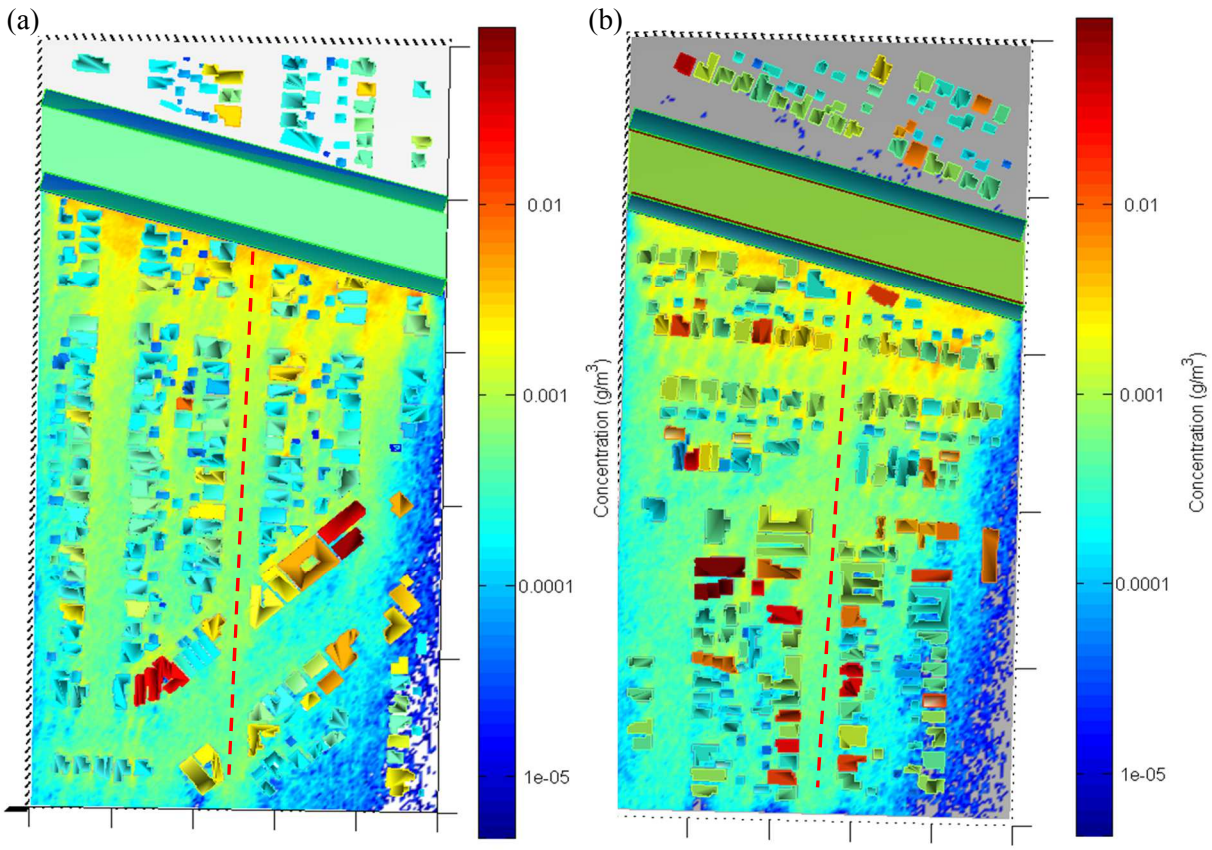

Fig. 33 The QUIC simulated particle concentrations for (a) vegetation-only barrier and (b) combination barrier sites near I-10 Santa Monica. The wind direction is perpendicular to the road and the wind speed at the reference height is 0.7 m/s. Horizontal concentration field at 1.5 m height is shown. Dash lines note the field measurement transects.

Along the two transects of interest, model output concentrations were averaged over a distance of 10 m crosswind, starting at 25 m downwind from the edge of the road. The concentration profiles at a 1.5 m height were used, corresponding to the height of the sample inlet for mobile measurements. The normalized particle concentration profiles for each transect is plotted together with the downwind distance from the road (Fig. 34). The QUIC simulated concentration profiles showed different reduction patterns downwind of different barriers. The concentration reduction behind the combination barrier was higher compared to the vegetation barrier for all wind speeds tested. This is in agreement with the field measurements at these sites

under moderate wind speeds, but not for low wind speeds (Fig. 22). The concentration difference between the sites generally reduced with increasing distance from the road, but this convergence was more pronounced at higher wind speeds. Under lower wind speeds, the pollution decay curves remained nearly parallel at 250 m away from the road. This is in agreement with the reduction pattern observed from field measurements at these sites (Fig. 22).

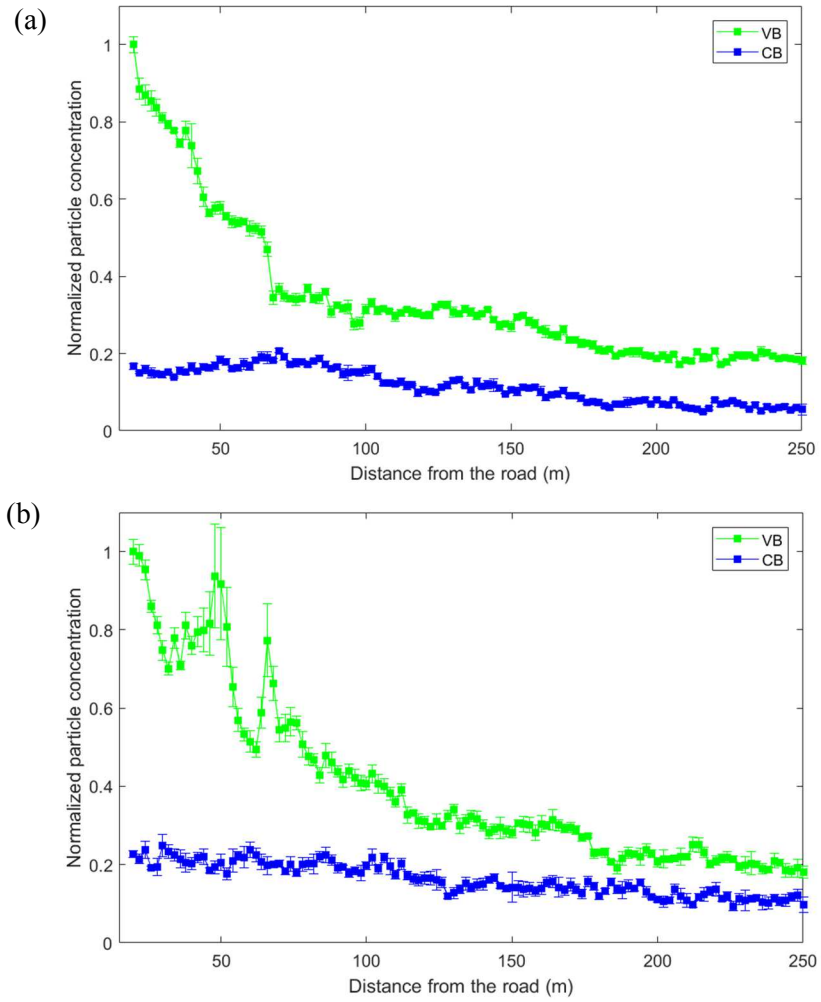

Fig. 34 The normalized particle concentration along two transects (VB: Vegetation-only barrier, CB: Combination barrier) at the I-10 Santa Monica site, under perpendicular wind conditions, from two different QUIC simulations. The wind speed at reference height is (a) 0.3 m/s and (b) 1.1 m/s. The mean concentration (symbol) is plotted together with the standard error (whiskers).

The relative concentration reduction percentage of a combination barrier, in comparison with the vegetation barrier was calculated using Eq. 5. Averaged over the first 160 m from the edge of the freeway, relative reduction percentages for QUIC simulated concentrations were, in general, higher than the relative reduction observed for field measurements.

Model simulations were conducted with different input wind speeds to probe the wind dependence of the relative concentration reduction percentage (Fig. 35). The simulated concentration field behind the barriers was not able to reproduce the observed wind dependence. The model does not include several mechanisms such as deposition and coagulation, by which UFP particles can be removed, especially by vegetation barriers. Therefore, the complex variations in particle deposition efficiencies at different wind speeds and for different particle sizes are not represented in the model. This could have contributed to the difference in wind speed dependence of the relative reductions calculated from field measurements and model results.

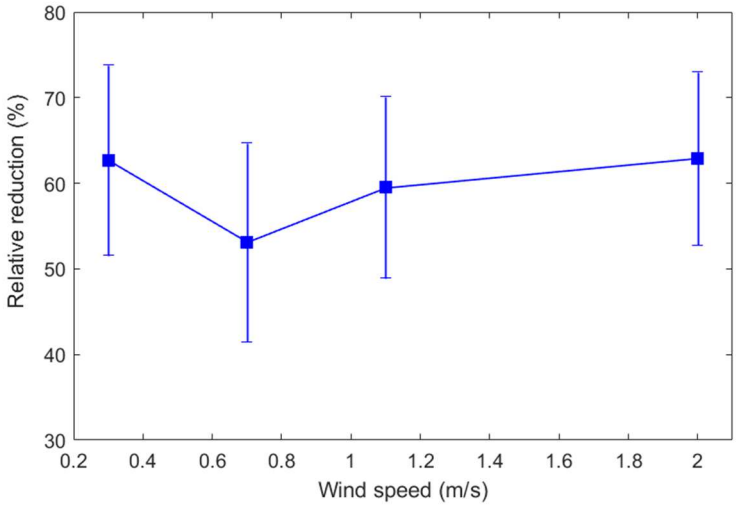

Fig. 35 The relative particle concentration reduction percentage (VEG-CB/VEG) as a function of the wind speed, under downwind conditions, averaged over the first 160 m from the edge of the freeway, from QUIC simulations for two sites near I-10 Santa Monica. Mean relative reduction is plotted together with the standard deviation.

These results suggests that the vegetation representation in the QUIC model can be improved by including a deposition model that incorporates vegetation characteristics related to the dynamic deposition efficiency of vegetation, such as the aerodynamic porosity/drag coefficient together with a vegetation density parameter (leaf-area density/leaf-area index/optical porosity).

5. Conclusions

The methodology proposed in chapter 2 produces concentration maps that preserve the valuable high spatial resolution of mobile monitoring data. By addressing the issues associated with non-uniform spatial resolution of measurements and the uncertainties associated with GPS data in a methodical and logical process, we are able to minimize the ambiguity of concentration maps. We showed that careful consideration should be given to all the factors influencing spatial resolution of underlying data; time resolution of the instruments, average speed of the MMP, post-data-processing procedures, when choosing an appropriate spatial resolution for producing average concentration maps. Adapting such a methodical data analysis for mobile monitoring data can facilitate straightforward and meaningful inter-comparison of concentration maps from different studies. The resulting high spatial resolution concentration maps provide a tool to identify pollution variations/hot spots at the block and sub-block scale, information that could be used to develop urban planning strategies to minimize pedestrian exposures in near-road environments.

The pollution concentration profiles developed from mobile measurements and presented in chapter 3 show that for roughly perpendicular winds, near-road elevated levels of ultrafine particle concentrations rapidly decrease within about 150 m and 500 m from the edge of the freeway, during daytime and early morning conditions, respectively. In general, for perpendicular winds, combination barriers resulted in lower pollution concentrations than a vegetation-only or sound wall-only barrier (Table 8). The largest benefit was observed closer to the barrier. Under daytime conditions, the combination barrier resulted in lower pollution concentrations downwind compared to the site with only a sound wall. However, at higher wind speeds the combination barrier became less effective, and was observed to increase pollutant

concentrations downwind, relative to a sound wall-only barrier, at the highest wind speed. In the calm early mornings, the taller and rather dense vegetation-only barrier was more effective than the combination barrier at very low wind speeds (<0.6 m/s), but at higher wind speeds the combination barrier was more effective. Similar to the daytime results, the combination barrier became less effective at highest wind speed. Under parallel wind conditions, when the freeway plume has a much smaller impact on pollutant concentrations in adjacent communities, pollution was elevated only slightly or not at all near the edge of the freeway. There was no detectable difference between sites with only vegetation only, sound wall only, or combination vegetation-solid wall barriers.

Table 8. Relative reductions[a] (%) of pollutants

Site: Session	**SM: calm (wind speed< 0.6 m/s)**		**SM: light winds (0.6 m/s<wind speed< 3 m/s)**		**SC**	
Pollutant	*Full*	*160 m*	*Full*	*160 m*	*Full*	*160 m*
UFP	-23	-24	16	25	7[b]	15[b]
$PM_{2.5}$	-22[c]	1[c]	31	33	< 1	< 1
PM_{10}	-5[c]	40[c]	26	30	n/a	n/a
NO	-26	-16	29	26	10	22
NO2	-31	-21	2	6	8	15
CO	-21	-10	17	15	n/a	n/a

[a] relative reduction as defined in Section 3.4.3
[b] average of only positive values
[c] only one day
n/a- data not available

This study indicates that in general, all three types of barriers considered; sound wall, vegetation and combination barriers, are effective near road air pollution mitigation strategies

that can be used by urban planners and policy makers. The combination barriers were found to provide the highest reduction under a large range wind speeds.

This study was able to find consistent results for pollution reduction by vegetation, across multiple urban sites. The careful selection of measurement sites, controlling for site characteristics that contribute to concentration differences, could have made this possible. The pollution reduction by vegetation barriers is strongly dependent on wind speed and density/optical porosity of the vegetation. Therefore, the results reported here could be limited to dense vegetation-only barriers and combination barriers with moderately dense vegetation. The choice of barrier can also be constrained by factors such as the cost, resources available for vegetation growth/maintenance. These limitations on effectiveness of vegetation barriers merit further research.

QUIC simulations presented in chapter 4, in general seem to capture the complex flow in near-road urban environments. The QUIC model show promise as a useful tool to optimize the characteristics of sound walls, vegetation barriers and combination barriers to mitigate near-road air pollution exposure and merit further improvements to handle characteristics of vegetation. Our results suggests that the vegetation representation in the QUIC model can be improved by including a deposition model that incorporates vegetation characteristics related to the dynamic deposition efficiency of vegetation, such as aerodynamic porosity/drag coefficient together with a vegetation density parameter (leaf-area density/leaf-area index/optical porosity).

Overall, this research adds to the growing body of scientific work that report large spatial variations of air pollution concentrations in near-road environments, and demonstrates how our understanding of these spatial gradients can facilitate mitigation strategies.

References

Abhijith, K. V., Kumar, P., Gallagher, J., McNabola, A., Baldauf, R., Pilla, F., et al. (2017). Air pollution abatement performances of green infrastructure in open road and built-up street canyon environments – A review. *Atmospheric Environment*, *162*, 71–86. https://doi.org/10.1016/j.atmosenv.2017.05.014

Al-Dabbous, A. N., & Kumar, P. (2014). The influence of roadside vegetation barriers on airborne nanoparticles and pedestrians exposure under varying wind conditions. *Atmospheric Environment*, *90*, 113–124. https://doi.org/10.1016/j.atmosenv.2014.03.040

Amini, S., Ahangar, F. E., Schulte, N., & Venkatram, A. (2016). Using models to interpret the impact of roadside barriers on near-road air quality. *Atmospheric Environment*, *138*, 55–64. https://doi.org/10.1016/j.atmosenv.2016.05.001

Baldauf, R., Thoma, E., Khlystov, A., Isakov, V., Bowker, G., Long, T., & Snow, R. (2008). Impacts of noise barriers on near-road air quality. *Atmospheric Environment*, *42*(32), 7502–7507. https://doi.org/10.1016/j.atmosenv.2008.05.051

Birmili, W., Rehn, J., Vogel, A., Boehlke, C., Weber, K., & Rasch, F. (2013). Micro-scale variability of urban particle number and mass concentrations in Leipzig, Germany [Text]. Retrieved May 29, 2018, from http://www.ingentaconnect.com/content/schweiz/mz/2013/00000022/00000002/art00007

Boothe, V. L., Boehmer, T. K., Wendel, A. M., & Yip, F. Y. (2014). Residential Traffic Exposure and Childhood Leukemia. *American Journal of Preventive Medicine*, *46*(4), 413–422. https://doi.org/10.1016/j.amepre.2013.11.004

Bowker, G. E., Baldauf, R., Isakov, V., Khlystov, A., & Petersen, W. (2007). The effects of roadside structures on the transport and dispersion of ultrafine particles from highways. *Atmospheric Environment*, *41*(37), 8128–8139. https://doi.org/10.1016/j.atmosenv.2007.06.064

Brantley, H. L., Hagler, G. S. W., J. Deshmukh, P., & Baldauf, R. W. (2014). Field assessment of the effects of roadside vegetation on near-road black carbon and particulate matter. *Science of The Total Environment*, *468–469*, 120–129. https://doi.org/10.1016/j.scitotenv.2013.08.001

Brantley, H. L., Hagler, G. S. W., Kimbrough, E. S., Williams, R. W., Mukerjee, S., & Neas, L. M. (2014). Mobile air monitoring data-processing strategies and effects on spatial air pollution trends. *Atmos. Meas. Tech.*, *7*(7), 2169–2183. https://doi.org/10.5194/amt-7-2169-2014

Brown, M., Nelson, M., D Williams, M., Gowardhan, A., & Pardyjak, E. (2010). A non-CFD modeling system for computing 3D wind and concentration fields in urban environments.

In *5th Int. Symp. Computational Wind Engineering (CWE2010). Chapel Hill, North Carolina*.

Caiazzo, F., Ashok, A., Waitz, I. A., Yim, S. H. L., & Barrett, S. R. H. (2013). Air pollution and early deaths in the United States. Part I: Quantifying the impact of major sectors in 2005. *Atmospheric Environment*, *79*, 198–208. https://doi.org/10.1016/j.atmosenv.2013.05.081

Chen, H., Goldberg, M. S., Burnett, R. T., Jerrett, M., Wheeler, A. J., & Villeneuve, P. J. (2013). Long-Term Exposure to Traffic-Related Air Pollution and Cardiovascular Mortality: *Epidemiology*, *24*(1), 35–43. https://doi.org/10.1097/EDE.0b013e318276c005

Chen, L., Liu, C., Zou, R., Yang, M., & Zhang, Z. (2016). Experimental examination of effectiveness of vegetation as bio-filter of particulate matters in the urban environment. *Environmental Pollution*, *208*, 198–208. https://doi.org/10.1016/j.envpol.2015.09.006

Chen, X., Pei, T., Zhou, Z., Teng, M., He, L., Luo, M., & Liu, X. (2015). Efficiency differences of roadside greenbelts with three configurations in removing coarse particles (PM10): A street scale investigation in Wuhan, China. *Urban Forestry & Urban Greening*, *14*(2), 354–360. https://doi.org/10.1016/j.ufug.2015.02.013

Choi, W., He, M., Barbesant, V., Kozawa, K. H., Mara, S., Winer, A. M., & Paulson, S. E. (2012). Prevalence of wide area impacts downwind of freeways under pre-sunrise stable atmospheric conditions. *Atmospheric Environment*, *62*, 318–327. https://doi.org/10.1016/j.atmosenv.2012.07.084

Choi, W., Hu, S., He, M., Kozawa, K., Mara, S., Winer, A. M., & Paulson, S. E. (2013). Neighborhood-scale air quality impacts of emissions from motor vehicles and aircraft. *Atmospheric Environment*, *80*, 310–321. https://doi.org/10.1016/j.atmosenv.2013.07.043

Choi, W., Ranasinghe, D., Bunavage, K., DeShazo, J. R., Wu, L., Seguel, R., et al. (2016). The effects of the built environment, traffic patterns, and micrometeorology on street level ultrafine particle concentrations at a block scale: Results from multiple urban sites. *Science of The Total Environment*, *553*, 474–485. https://doi.org/10.1016/j.scitotenv.2016.02.083

Choi, W., Ranasinghe, D., DeShazo, J. R., Kim, J.-J., & Paulson, S. E. (2018). Where to locate transit stops: Cross-intersection profiles of ultrafine particles and implications for pedestrian exposure. *Environmental Pollution*, *233*, 235–245. https://doi.org/10.1016/j.envpol.2017.10.055

Durant, J. L., Ash, C. A., Wood, E. C., Herndon, S. C., Jayne, J. T., Knighton, W. B., et al. (2010). Short-term variation in near-highway air pollutant gradients on a winter morning. *Atmospheric Chemistry and Physics (Print)*, *10*(2), 5599–5626.

Fantozzi, F., Monaci, F., Blanusa, T., & Bargagli, R. (2015). Spatio-temporal variations of ozone and nitrogen dioxide concentrations under urban trees and in a nearby open area. *Urban Climate*, *12*(2), 119–127. https://doi.org/10.1016/j.uclim.2015.02.001

Fernando, H. J. S., Zajic, D., Di Sabatino, S., Dimitrova, R., Hedquist, B., & Dallman, A. (2010). Flow, turbulence, and pollutant dispersion in urban atmospheres. *Physics of Fluids*, *22*(5), 51301. https://doi.org/10.1063/1.3407662

Finn, D., Clawson, K. L., Carter, R. G., Rich, J. D., Eckman, R. M., Perry, S. G., et al. (2010). Tracer studies to characterize the effects of roadside noise barriers on near-road pollutant dispersion under varying atmospheric stability conditions. *Atmospheric Environment*, *44*(2), 204–214. https://doi.org/10.1016/j.atmosenv.2009.10.012

Fritsch, F., & Carlson, R. (1980). Monotone Piecewise Cubic Interpolation. *SIAM Journal on Numerical Analysis*, *17*(2), 238–246. https://doi.org/10.1137/0717021

Fujii, E., Lawton, J., Cahill, T. A., Barnes, D. E., Hayes, C., & Spada, N. (2008). *Removal Rates of Particulate Matter onto Vegetation as a Function of Particle Size* (Final Report to Breathe California of Sacramento.). Breathe California of Sacramento-Emigrant Trails' Health Effects Task Force (HETF) and Sacramento Metropolitan Air Quality Management District.

Ghasemian, M., Amini, S., & Princevac, M. (2017). The influence of roadside solid and vegetation barriers on near-road air quality. *Atmospheric Environment*, *170*, 108–117. https://doi.org/10.1016/j.atmosenv.2017.09.028

Hagler, G. S. W., Thoma, E. D., & Baldauf, R. W. (2010). High-Resolution Mobile Monitoring of Carbon Monoxide and Ultrafine Particle Concentrations in a Near-Road Environment. *Journal of the Air & Waste Management Association*, *60*(3), 328–336. https://doi.org/10.3155/1047-3289.60.3.328

Hagler, G. S. W., Tang, W., Freeman, M. J., Heist, D. K., Perry, S. G., & Vette, A. F. (2011). Model evaluation of roadside barrier impact on near-road air pollution. *Atmospheric Environment*, *45*(15), 2522–2530. https://doi.org/10.1016/j.atmosenv.2011.02.030

Hagler, G. S. W., Lin, M.-Y., Khlystov, A., Baldauf, R. W., Isakov, V., Faircloth, J., & Jackson, L. E. (2012). Field investigation of roadside vegetative and structural barrier impact on near-road ultrafine particle concentrations under a variety of wind conditions. *Science of The Total Environment*, *419*, 7–15. https://doi.org/10.1016/j.scitotenv.2011.12.002

Health Effects Institute Panel on the Health Effects of Traffic-Related Air Pollution. (2010). *Traffic-related air pollution: a critical review of the literature on emissions, exposure, and health effects*. Health Effects Institute.

Heist, D. K., Perry, S. G., & Brixey, L. A. (2009). A wind tunnel study of the effect of roadway configurations on the dispersion of traffic-related pollution. *Atmospheric Environment*, *43*(32), 5101–5111. https://doi.org/10.1016/j.atmosenv.2009.06.034

Hinds, W. C. (1999). *Aerosol Technology: Properties, Behavior, and Measurement of Airborne Particles* (2nd Edition).

Hölscher, N., Höffer, R., Niemann, H.-J., Brilon, W., & Romberg, E. (1993). Wind tunnel experiments on micro-scale dispersion of exhausts from motorways. *Science of The Total Environment*, *134*(1–3), 71–79. https://doi.org/10.1016/0048-9697(93)90340-C

Hu, S., Fruin, S., Kozawa, K., Mara, S., Paulson, S. E., & Winer, A. M. (2009). A wide area of air pollutant impact downwind of a freeway during pre-sunrise hours. *Atmospheric Environment*, *43*(16), 2541–2549. https://doi.org/10.1016/j.atmosenv.2009.02.033

Hu, S., Paulson, S. E., Fruin, S., Kozawa, K., Mara, S., & Winer, A. M. (2012). Observation of elevated air pollutant concentrations in a residential neighborhood of Los Angeles California using a mobile platform. *Atmospheric Environment*, *51*, 311–319. https://doi.org/10.1016/j.atmosenv.2011.12.055

Karner, A. A., Eisinger, D. S., & Niemeier, D. A. (2010). Near-Roadway Air Quality: Synthesizing the Findings from Real-World Data. *Environmental Science & Technology*, *44*(14), 5334–5344. https://doi.org/10.1021/es100008x

Kent, C. W., Grimmond, S., & Gatey, D. (2017). Aerodynamic roughness parameters in cities: Inclusion of vegetation. *Journal of Wind Engineering and Industrial Aerodynamics*, *169*, 168–176. https://doi.org/10.1016/j.jweia.2017.07.016

Kumar, P., Ketzel, M., Vardoulakis, S., Pirjola, L., & Britter, R. (2011). Dynamics and dispersion modelling of nanoparticles from road traffic in the urban atmospheric environment—A review. *Journal of Aerosol Science*, *42*(9), 580–603. https://doi.org/10.1016/j.jaerosci.2011.06.001

Lähde, T., Niemi, J. V., Kousa, A., Rönkkö, T., Karjalainen, P., Keskinen, J., et al. (2014). Mobile Particle and NOx Emission Characterization at Helsinki Downtown: Comparison of Different Traffic Flow Areas. *Aerosol and Air Quality Research*, *14*(5), 1372–1382. https://doi.org/10.4209/aaqr.2013.10.0311

Lee, E. S., Ranasinghe, D. R., Ahangar, F. E., Amini, S., Mara, S., Choi, W., et al. (2018). Field evaluation of vegetation and noise barriers for mitigation of near-freeway air pollution under variable wind conditions. *Atmospheric Environment*, *175*, 92–99. https://doi.org/10.1016/j.atmosenv.2017.11.060

Lin, M.-Y., & Khlystov, A. (2012). Investigation of Ultrafine Particle Deposition to Vegetation Branches in a Wind Tunnel. *Aerosol Science and Technology*, *46*(4), 465–472. https://doi.org/10.1080/02786826.2011.638346

Lin, M.-Y., Hagler, G., Baldauf, R., Isakov, V., Lin, H.-Y., & Khlystov, A. (2016). The effects of vegetation barriers on near-road ultrafine particle number and carbon monoxide concentrations. *Science of The Total Environment*, *553*, 372–379. https://doi.org/10.1016/j.scitotenv.2016.02.035

Misra, P., & Enge, P. (2006). *Global Positioning System: Signals, Measurements, and Performance* (Second Edition). Ganga-Jamuna Press, Lincoln (MA), U.S.A.

Morakinyo, T. E., Lam, Y. F., & Hao, S. (2016). Evaluating the role of green infrastructures on near-road pollutant dispersion and removal: Modelling and measurement. *Journal of Environmental Management*, *182*, 595–605. https://doi.org/10.1016/j.jenvman.2016.07.077

Ning, Z., Hudda, N., Daher, N., Kam, W., Herner, J., Kozawa, K., et al. (2010). Impact of roadside noise barriers on particle size distributions and pollutants concentrations near freeways. *Atmospheric Environment*, *44*(26), 3118–3127. https://doi.org/10.1016/j.atmosenv.2010.05.033

Padró-Martínez, L. T., Patton, A. P., Trull, J. B., Zamore, W., Brugge, D., & Durant, J. L. (2012). Mobile monitoring of particle number concentration and other traffic-related air pollutants in a near-highway neighborhood over the course of a year. *Atmospheric Environment*, *61*, 253–264. https://doi.org/10.1016/j.atmosenv.2012.06.088

Pardyjak, E. R., & Brown, M. J. (2007, April 27). QUIC URB v. 1.1 Theory and Users Guide. Los Alamos National Laboratory.

Pattinson, W., Longley, I., & Kingham, S. (2014). Using mobile monitoring to visualise diurnal variation of traffic pollutants across two near-highway neighbourhoods. *Atmospheric Environment*, *94*, 782–792. https://doi.org/10.1016/j.atmosenv.2014.06.007

Peters, J., Theunis, J., Poppel, M. V., & Berghmans, P. (2013). Monitoring PM10 and Ultrafine Particles in Urban Environments Using Mobile Measurements. *Aerosol and Air Quality Research*, *13*(2), 509–522. https://doi.org/10.4209/aaqr.2012.06.0152

Peters, J., Van den Bossche, J., Reggente, M., Van Poppel, M., De Baets, B., & Theunis, J. (2014). Cyclist exposure to UFP and BC on urban routes in Antwerp, Belgium. *Atmospheric Environment*, *92*, 31–43. https://doi.org/10.1016/j.atmosenv.2014.03.039

Petroff, A., Mailliat, A., Amielh, M., & Anselmet, F. (2008). Aerosol dry deposition on vegetative canopies. Part II: A new modelling approach and applications. *Atmospheric Environment*, *42*(16), 3654–3683. https://doi.org/10.1016/j.atmosenv.2007.12.060

Pirjola, L., Lähde, T., Niemi, J. V., Kousa, A., Rönkkö, T., Karjalainen, P., et al. (2012). Spatial and temporal characterization of traffic emissions in urban microenvironments with a mobile laboratory. *Atmospheric Environment*, *63*, 156–167. https://doi.org/10.1016/j.atmosenv.2012.09.022

Ranasinghe, D. R., Choi, W., Winer, A. M., & Paulson, S. E. (2016). Developing High Spatial Resolution Concentration Maps Using Mobile Air Quality Measurements. *Aerosol and Air Quality Research*, *16*(8), 1841–1853. https://doi.org/10.4209/aaqr.2015.07.0484

Rice, M. B., Rifas-Shiman, S. L., Oken, E., Gillman, M. W., Ljungman, P. L., Litonjua, A. A., et al. (2014). Exposure to traffic and early life respiratory infection: A cohort study. *Pediatric Pulmonology*. https://doi.org/10.1002/ppul.23029

Steffens, J. T., Wang, Y. J., & Zhang, K. M. (2012a). Exploration of effects of a vegetation barrier on particle size distributions in a near-road environment. *Atmospheric Environment*, *50*, 120–128. https://doi.org/10.1016/j.atmosenv.2011.12.051

Stingone, J. A., Luben, T. J., Daniels, J. L., Fuentes, M., Richardson, D. B., Aylsworth, A. S., et al. (2014). Maternal Exposure to Criteria Air Pollutants and Congenital Heart Defects in Offspring: Results from the National Birth Defects Prevention Study. *Environmental Health Perspectives*, *122*(8), 863–872. https://doi.org/10.1289/ehp.1307289

Tong, Z., Whitlow, T. H., MacRae, P. F., Landers, A. J., & Harada, Y. (2015). Quantifying the effect of vegetation on near-road air quality using brief campaigns. *Environmental Pollution*, *201*, 141–149. https://doi.org/10.1016/j.envpol.2015.02.026

Van den Bossche, J., Peters, J., Verwaeren, J., Botteldooren, D., Theunis, J., & De Baets, B. (2015). Mobile monitoring for mapping spatial variation in urban air quality: Development and validation of a methodology based on an extensive dataset. *Atmospheric Environment*, *105*, 148–161. https://doi.org/10.1016/j.atmosenv.2015.01.017

Van Poppel, M., Peters, J., & Bleux, N. (2013). Methodology for setup and data processing of mobile air quality measurements to assess the spatial variability of concentrations in urban environments. *Environmental Pollution*, *183*, 224–233. https://doi.org/10.1016/j.envpol.2013.02.020

Wang, H., Takle, E. S., & Shen, and J. (2001). SHELTERBELTS AND WINDBREAKS: Mathematical Modeling and Computer Simulations of Turbulent Flows. *Annual Review of Fluid Mechanics*, *33*(1), 549–586. https://doi.org/10.1146/annurev.fluid.33.1.549

Zhang, K. M., Wexler, A. S., Zhu, Y. F., Hinds, W. C., & Sioutas, C. (2004). Evolution of particle number distribution near roadways. Part II: the "Road-to-Ambient" process. *Atmospheric Environment*, *38*(38), 6655–6665. https://doi.org/10.1016/j.atmosenv.2004.06.044

Zhu, Y., Hinds, W. C., Kim, S., Shen, S., & Sioutas, C. (2002). Study of ultrafine particles near a major highway with heavy-duty diesel traffic. *Atmospheric Environment*, *36*(27), 4323–4335. https://doi.org/10.1016/S1352-2310(02)00354-0

Zwack, L. M., Hanna, S. R., Spengler, J. D., & Levy, J. I. (2011). Using advanced dispersion models and mobile monitoring to characterize spatial patterns of ultrafine particles in an urban area. *Atmospheric Environment*, *45*(28), 4822–4829. https://doi.org/10.1016/j.atmosenv.2011.06.019